

# Wind 2013 Senior Review Proposal

Adam Szabo  
NASA GSFC  
Project Scientist/Presenter

Lynn B. Wilson III  
NASA GSFC  
Deputy Project Scientist

## Executive Summary

NASA launched the *Wind* spacecraft in November, 1994 to the Earth's L1 Lagrange point as the interplanetary component of the Global Geospace Science Program within the International Solar Terrestrial Physics (ISTP) program. The spin stabilized spacecraft – spin axis aligned with ecliptic south – carries eight instrument suites that provide comprehensive measurements of thermal particles to solar energetic particles, quasi-static fields to high frequency radio waves, and  $\gamma$ -rays. All of the instrument suites continue to provide valuable scientific observations completely available to the public (except the TGRS  $\gamma$ -ray instrument, now without coolant).

The *Wind* instrument suite provides comprehensive and unique high time resolution (HTR) in-situ solar

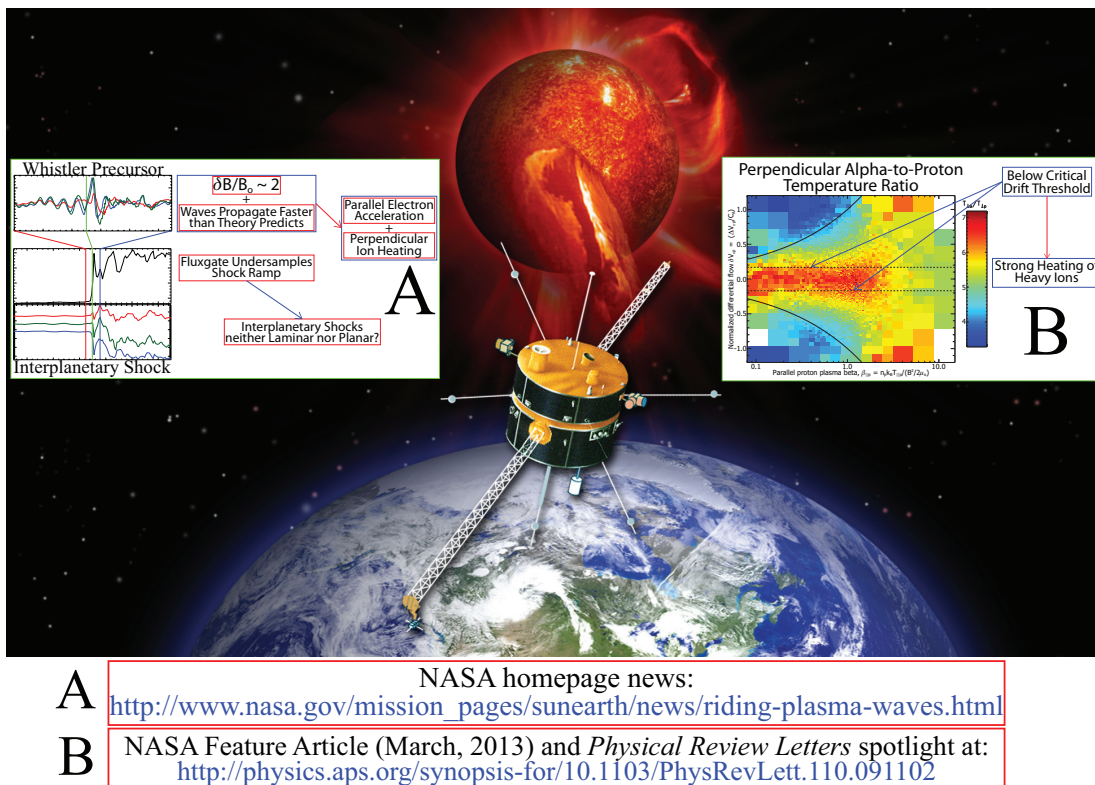


**Figure 1:** *Wind*, a comprehensive solar wind monitor in the news. For detailed explanations of the insets, see Section 2.1.1.

wind measurements that enable the investigation of wave-particle interactions. *Wind* is the only near-Earth spacecraft equipped with radio waves instrumentation. *Wind* has made numerous independent discoveries since the last senior review, from constraining theories of solar wind heating to direct observations of wave-driven particle acceleration and heating (see insets in Figure 1). *Wind* data have been critical to a wide range of studies resulting in **~480 refereed publications between 2010-2012** (e.g., since the last Senior Review) and **~2800 refereed publications since launch** (listed on the *Wind* project Web page: <http://wind.nasa.gov>). **Since 2009, 10 graduate students received doctoral degrees using *Wind* observations.** The new results span all three heliophysics research objectives as described in the *Science Plan for NASA's Science Mission Directorate 2007-2016*. The *Wind* science data products are publicly served directly from the instrument team sites and CDAWeb, with a single project web page containing links to and descriptions of the large number of *Wind* data products. *Wind* is also an active participant in the development of the Virtual Heliophysics Observatory (VHO) that allows for more complex queries.

Even though *Wind* is >18 years old, the spacecraft is still in good health and promises a host of new discoveries. The time period covered by this proposal includes the next solar maximum and its decline. Because of its longevity, *Wind* observations will allow researchers to compare solar wind properties between solar cycles 22,

23 and 24 without needing to compensate for changing instrumentation and calibration. Furthermore, new *Wind* data, recalibrated this past year and already resulting in new discoveries, will **provide unprecedentedly accurate and high time, energy, and angular resolution measurements of the near-Earth 1 AU solar wind.**

*Wind* has also contributed critically to multi-mission studies, as part of the Heliophysics System Observatory (HSO). With its ample fuel reserves, sufficient for ~60 years, *Wind* will continue to provide accurate solar wind input for magnetospheric studies (supporting MMS and *Van Allen Probes*) and serve as the 1 AU reference point for both inner heliospheric (e.g., MESSENGER) and outer heliospheric (e.g., *Voyager*) investigations, in addition to providing critical support for other NASA missions (e.g., STEREO, ACE, etc.). Moreover, new *Wind* results will continue to improve theories of solar wind heating, acceleration, and energetic particle processes to focus the science objectives of future missions (e.g., *Solar Probe Plus* and *Solar Orbiter*). Once these new missions are launched, ***Wind* will provide critical measurements to complement the observations made by *Solar Probe Plus* and *Solar Orbiter* enabling the connection of the 1 AU solar wind to its coronal source and comparison of radio burst power and source locations.**

**Rationale for Continuing the *Wind* Mission**

- *Wind* continues to provide unique, robust, and high resolution solar wind measurements
- *Wind* will provide HTR measurements serving as the 1 AU reference for *Solar Probe Plus* and *Solar Orbiter*
- *Wind* is a 3rd solar wind and radio vantage point with STEREO, providing uniform 1AU ecliptic coverage
- *Wind* and ACE together can provide 24/7 near-Earth L1 monitoring for the next  $\gtrsim 10$  years
- *Wind* and ACE are complementary not identical  $\Rightarrow$  both are needed for complete 1 AU baseline observations
- *Wind* still has redundant systems, instruments, and enough fuel for 60 years
- *Wind*'s scientific productivity remains high  $\rightarrow$  significant discoveries in all three SMD research objectives

**Table of Contents**

<b>Executive Summary</b>	<b>1</b>
<b>1 Science and Science Implementation</b>	<b>3</b>
1.1 Historical Background . . . . .	3
1.2 Current Status . . . . .	3
1.3 <i>Wind</i> 's Unique Capabilities . . . . .	3
1.4 Heliophysics System Observatory . . . . .	4
<b>2 Recent Accomplishments</b>	<b>5</b>
2.1 Heliophysics Objective #1: Fundamental Physical Processes . . . . .	5
2.2 Heliophysics Objective #2: Evolution of Solar Transients in the Heliosphere . . . . .	11
2.3 Heliophysics Objective #3: Solar Cycle Variations . . . . .	16
<b>3 Prioritized Science Goals</b>	<b>18</b>
3.1 Two Complete Solar Cycles . . . . .	19
3.2 Solar Wind Heating and Kinetic Physics . . . . .	19
3.3 The Evolution of ICMEs . . . . .	20
3.4 Dust Science . . . . .	21
<b>4 <i>Wind</i> Support for Current and Future Missions</b>	<b>21</b>
4.1 <i>Wind</i> and ACE, DSCOVR, and STEREO . . . . .	21
4.2 <i>Wind</i> and MESSENGER, VEX, and MAVEN . . . . .	22
4.3 <i>Wind</i> and <i>Solar Probe Plus</i> and <i>Solar Orbiter</i> . . . . .	22
4.4 <i>Wind</i> and IBEX and <i>Voyagers</i> . . . . .	22
4.5 <i>Wind</i> and <i>Van Allen Probes</i> , MMS, THEMIS, and <i>Cluster</i> . . . . .	23
4.6 <i>Wind</i> and RHESSI and <i>Swift</i> and <i>Fermi</i> . . . . .	23
4.7 <i>Wind</i> and CCMC . . . . .	23
<b>5 Technical Status and Budget</b>	<b>24</b>
5.1 Spacecraft Health . . . . .	24
5.2 Instrument Status . . . . .	24
5.3 Science Team . . . . .	24
5.4 Ground Operations . . . . .	25
5.5 In-Guide Budget . . . . .	26
<b>References</b>	<b>27</b>
<b>A Mission Archive Plan</b>	<b>31</b>
<b>B Education and Public Outreach</b>	<b>38</b>
<b>Acronyms and Initialisms</b>	<b>41</b>
<b>Budget Spreadsheet</b>	<b>44</b>

## 1 Science and Implementation

### 1.1 Historical Background

The *Wind* spacecraft was launched in November, 1994 as the interplanetary component of the Global Geospace Science (GGS) Program within ISTP. *Wind*'s original purpose was (1) to make accurate in-situ measurements of interplanetary conditions upstream of the magnetosphere to complement measurements made in the magnetosphere by *Polar* and *Geotail* and (2) to remotely sense interplanetary disturbances for possible future predictive purposes. The instruments were therefore designed to make highly accurate solar wind measurements.

After a number of years at the L1 Lagrange point, *Wind* performed a series of orbital maneuvers to take it to various scientifically valuable observational points. In 1999, *Wind* executed a number of magnetospheric petal orbits that took it to the rarely sampled geomagnetic high latitudes. Between 2000 and 2002, *Wind* moved further and further away from the Sun-earth line (and ACE) reaching 350  $R_E$  to the side in a distant prograde orbit. Finally, in 2003, it completed an L2 campaign taking the spacecraft more than 250  $R_E$  downstream of Earth and  $\sim 500 R_E$  downstream of ACE to investigate solar wind evolution and magnetotail phenomena. Since 2004, *Wind* has remained at L1 where it will stay for the foreseeable future.

### 1.2 Current Status

The *Wind* spacecraft continues to operate in good health. In 2000, the team successfully reconfigured the communications system to enhance the telemetry margin. Reliance on a single digital tape recorder since 1997 has never hampered operations, and the team took measures to minimize its use in order to extend tape recorder life as long as possible.

Seven of the eight *Wind* instruments, including all of the particles and fields instruments, remain largely or fully operational. The EPACT, high energy particle, and SMS solar wind composition instruments suffered some degradation, but both continue to provide valuable measurements. The SWE electron instrument required some reconfiguration to maintain its capabilities and the TGRS  $\gamma$ -ray detector has been turned off, as planned due to it no longer having sufficient coolant to operate. For technical details see Section 5.2. All the other instruments operate nominally. Thus, the net loss in capability remains minimal and the *Wind* instruments continue to provide definitive and continuous measurements of the solar wind.

In conclusion, *Wind* is operationally healthy and continues to maintain a large fuel reserve, capable of sustaining the spacecraft at L1 for almost 60 years.

### 1.3 *Wind*'s Unique Capabilities

*Wind*'s complement of instruments was optimized for studies of solar wind plasma, interplanetary magnetic field, radio and plasma waves, and of low energetic particles. The instrument suite is not equivalent to that on ACE, rather the two missions complement each other. ACE – launched a few years after *Wind* – focuses on the detailed investigation of high energy particles for which *Wind* has limited capabilities. Therefore, several of the *Wind* solar wind, suprathermal particle, and especially radio and plasma wave instruments are unique. *Wind*'s instrument capabilities are summarized in Table 1 and are compared to ACE and STEREO. ***Wind is unparalleled for low energy particle and radio wave observations of the solar wind for near-Earth spacecraft.*** A more detailed discussion of the unique *Wind* capabilities follows in the next paragraphs.

Collaborating with STEREO, *Wind*/WAVES provides an essential third vantage point along the Sun-Earth line, allowing the unambiguous localization of inner heliospheric radio sources and the determination of their corresponding beam patterns. More importantly, *Wind* is the only spacecraft at L1 that can observe the thermal noise regime of the plasma, which provides the most accurate measurement of the local electron plasma frequency in the solar wind. This quantity is directly proportional to the square root of the electron number density. Thus, the density – normally obtained as a moment or fit of the velocity distribution function from particle instruments like SWE and 3DP – can be accurately and independently derived from the WAVES instrument. The WAVES instrument provides the only method for an independent, in-flight, and absolute calibration for particle instruments for spacecraft near L1.

*Wind* is unique in its capacity for high time resolution (HTR) measurements of quasi-static magnetic fields (MFI instrument) and thermal solar wind electrons (3DP). Though STEREO/SWEA has a higher cadence in burst mode, the low energy ( $\lesssim 60$  eV) electrons are contaminated causing *Wind*/3DP to have the highest time resolution measurements of thermal electrons. *Wind*/MFI offers continuous coverage of the quasi-static magnetic fields at  $\sim 11$  samples per second (sps) over the entire mission ( $\sim 22$  sps when *Wind* was within  $\lesssim 100 R_E$  of Earth), still the highest sample rate of continuous solar wind measurements.

*Wind*/STICS is unique among currently operational spacecraft as it is the only sensor in space fully dedicated to providing measurements of heavy ions for an energy range spanning  $\sim 6.2$ –223.1 keV/amu. As STICS is a time-of-flight mass spectrometer, it can differentiate many minor ionic species and look at their characteristics in the suprathermal energy range to better understand their origin. In addition, *Wind*/LEMT provides high energy particle data over a range of en-

**Table 1:** The measurement capabilities of *Wind* compared to STEREO and ACE

Type	<i>Wind</i>	STEREO	ACE	Comments for <i>Wind</i>
DC Magnetic Field	MFI ~11 sps <sup>a</sup>	MAG ~8 sps, (~32 sps burst)	MAG ~6 sps	highest time resolution for continuous coverage
Radio Waves	WAVES ~4kHz–14MHz	S/WAVES ~2.5kHz–16MHz	N/A	unique large antenna length allows for measurement of local plasma frequency → electron density
Time Domain Waveforms	TDS ~1.9–120ksps <sup>b</sup>	TDS ~7.8–250ksps	N/A	search coil and long antenna → better calibration and more sensitive
Thermal Ions (Moments)	3DP <sup>c</sup> SWE ~92 s	PLASTIC ~60 s	SWEPAM ~64 s	highest time, angular, and energy resolution; robust and redundant; operates during solar storms
Thermal Ions (DFs <sup>d</sup> )	3DP ~24 s <sup>e</sup>	PLASTIC N/A	SWEPAM N/A	highest time, angular, and energy resolution
Thermal Electrons (Moments)	3DP (~3 s) SWE (~9 s)	SWEA <sup>f</sup> (~2 s)	SWEPAM (~128 s)	highest time resolution for full $4\pi$ coverage at low energy
Thermal Electrons (DFs)	3DP ~3 s	SWEA ~2 s	SWEPAM N/A	[same as above]
Solar Wind Composition	SMS/STICS $1 \leq Z \leq 56$ ~0.3–230keV/Q	PLASTIC $1 \leq Z \leq 56$ ~0.3–80keV/Q	SWICS $1 \leq Z \leq 30$ ~0.5–100keV/Q	only observations > 100 keV/Q
Mass Spectrometry	SMS/MASS $1 \leq Z \leq 28$ ~0.5–12keV/Q	N/A N/A N/A	SWIMS $2 \leq Z \leq 30$ ~0.5–20keV/Q	comparable to ACE in both charge and energy
Low Energy Electrons	3DP ~3eV–500keV	SWEA <sup>g</sup> SEPT <sup>h</sup> STE <sup>i</sup>	SWEPAM EPAM ~3eV–400keV	full 3D measurements from a few eV to ~500 keV
Low Energy Ions	3DP ~3eV–7MeV	SEPT ~60keV–7MeV	SWEPAM <sup>j</sup> EPAM <sup>k</sup> ULEIS <sup>l</sup>	measurements of solar wind thermal core to lower energies
High Energy Particles	EPACT/LEMT ~0.04–50MeV/n	SIT <sup>m</sup> LET <sup>n</sup> HET <sup>o</sup>	SIS CRIS ~10–600MeV/n	robust; high geometry factor; unique directional observations; and energy range

<sup>a</sup> ~22 samples per second when inside 100  $R_E$ ; <sup>b</sup> kilosamples per second; <sup>c</sup> moments: ~3s, distributions: ~24s, burst: ~3s; <sup>d</sup> DF = velocity distribution function; <sup>e</sup> ~3s in burst mode; <sup>f</sup> nothing below ~60eV; <sup>g</sup> ~60–3000eV; <sup>h</sup> ~2–100keV, 4/8 telescopes contaminated; <sup>i</sup> ~30–400keV; <sup>j</sup> ~260eV–35keV; <sup>k</sup> ~46–4800keV; <sup>l</sup> ~45keV/n–2MeV/n; <sup>m</sup> ~0.03–5MeV/n; <sup>n</sup> ~2–60MeV/n; <sup>o</sup> ~1–170MeV/n;

ergies not covered by ACE.

#### 1.4 Heliophysics System Observatory

*Wind* plays an active role in the Heliophysics System Observatory (HSO). *Wind* achieved many of its recent scientific discoveries in collaboration with other spacecraft as described in more detail in Section 2 below. However, the HSO is more than just the occasional comparison of data from multiple platforms. It is a data environment where such comparisons can be readily performed. As the Heliophysics Data Policy outlines, this data environment requires the presence of in-depth metadata for each data product based on a

uniform standard (the SPASE dictionary). It also envisions the eventual connection of the current distributed data repositories by a number of virtual observatories enabling the location and downloading of the desired data. *Wind* plays a leadership role in the deployment of the Virtual Heliospheric Observatory (VHO), the heliospheric portion of this environment, and the generation of the corresponding metadata.

The Living With a Star (LWS) program seeks to better understand the Sun-Earth connected system with the aim of developing reliable space weather forecasting capabilities. The program architecture plan calls

for a near-Earth solar wind monitor to connect the solar (SDO) and inner heliospheric (*Solar Probe Plus* and *Solar Orbiter*) observations with geomagnetic ones (*Van Allen Probes*). However, NASA has no current plans for a new solar wind and Solar Energetic Particle (SEP) monitoring mission, rather NASA assumes that *Wind*, ACE or both will survive into the 2013-2022 time frame. The lowest risk option to satisfy the near-Earth solar wind monitoring requirement of LWS is to sustain both *Wind* and ACE – either of which can satisfy the LWS measurement requirements – because both are well past their prime missions and design lifetimes. Again, note that *Wind* and ACE are not duplicate spacecraft but rather serve complementary roles. Thus, the most prudent course of action involves preserving both spacecraft.

## 2 Recent Accomplishments

The great unanswered questions of heliophysics are: (1) what heats the corona; (2) what accelerates the solar wind; and (3) what are the physical processes that produce SEPs. Two upcoming missions are dedicated to resolving these outstanding issues: *Solar Probe Plus* and *Solar Orbiter*. Both of these new missions will head to the inner heliosphere where their observations will be significantly limited by telemetry constraints and by the large solar heat flux that makes sunward-pointing particle telescopes difficult to operate.

However, the solar wind carries to 1 AU telltale signs of its origin and of the critical processes that accelerate particles. Thus, the unique full sky  $4\pi$  steradian particle and high time resolution comprehensive fields observations from *Wind* have resulted in a steady stream of discoveries during the past years constraining solar wind and SEP theories and models. In collaboration with STEREO and ACE, *Wind* has also significantly contributed to our understanding of ICME structures, efforts to predict their arrival at 1 AU, and the global properties of the heliosphere during the current unusually long solar minimum. Finally, *Wind* remains a critical source of solar wind input for Earth magnetospheric studies.

This section highlights recent *Wind* discoveries organizing them along the three heliophysics research objective areas. Moreover, it demonstrates that as a result of newly developed theories and models, and due to improved instrument data production and analysis, *Wind* will continue to contribute significantly to new discoveries and understanding of the origin and structure of the solar wind and of the acceleration, transport, and modulation of SEPs. Our detailed science plans for the FY2014-FY2018 period are outlined in Section 3.

### 2.1 Heliophysics Objective #1

The first heliophysics research objective, as articulated by the *Science Plan for NASA's Science Mission*

*Directorate 2007-2016*, is to understand the fundamental physical processes of the space environment from the Sun to Earth. *Wind* observations were key to making progress in two of the focus areas of this objective: (1) understanding the plasma processes that accelerate and transport both the solar wind and energetic particles; and (2) understanding magnetic reconnection.

#### 2.1.1 Solar Wind Acceleration and Heating

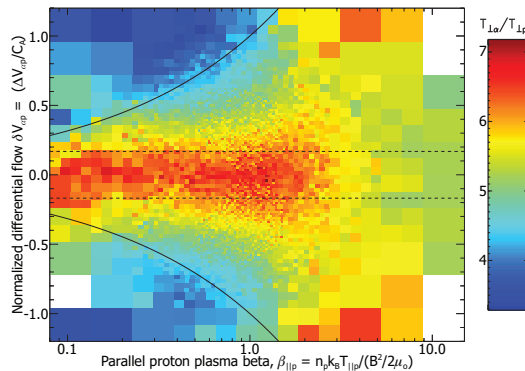


**Figure 2:** *Kasper et al.* [Adapted from Figure 2 in 2013].

A major challenge in heliophysics is to identify the processes responsible for heating the solar corona and the solar wind. A recent study by *Kasper et al.* [2013], using the stable and long duration *Wind* Faraday Cup measurements, demonstrated that a very specific ion heating mechanism is acting in a combination of the corona and the solar wind. The theory of wave-particle resonance of cyclotron waves propagating in opposite directions predicts that helium and heavier ions can be strongly heated as long as their differential speed relative the bulk proton solar wind flow does not exceed a critical value. Demonstration of this effect [*Kasper et al.*, 2007] required statistically significant numbers of low collisional age plasma, which could only be obtained from a data set with millions of independent solar wind observations.

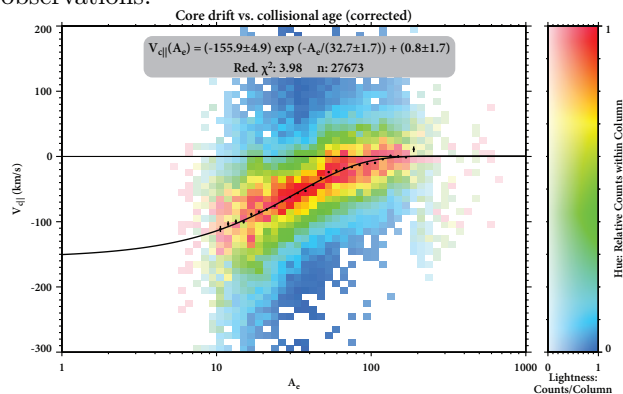


**Figure 3:** Corrected core electron drift velocity  $V_{c||}$  plotted as a function of collisional age  $A_e$ , binned in columns of  $A_e$  and rows of  $V_{c||}$  ( $V_{c||} < 0$  corresponds to a sunward core drift). The black dots represent the average  $V_{c||}$  in each column. The solid black line shows the fit results [*Pulupa et al.*, 2013].

Specifically, in Figure 2, the helium ions are heated by over seven times more than the solar wind pro-

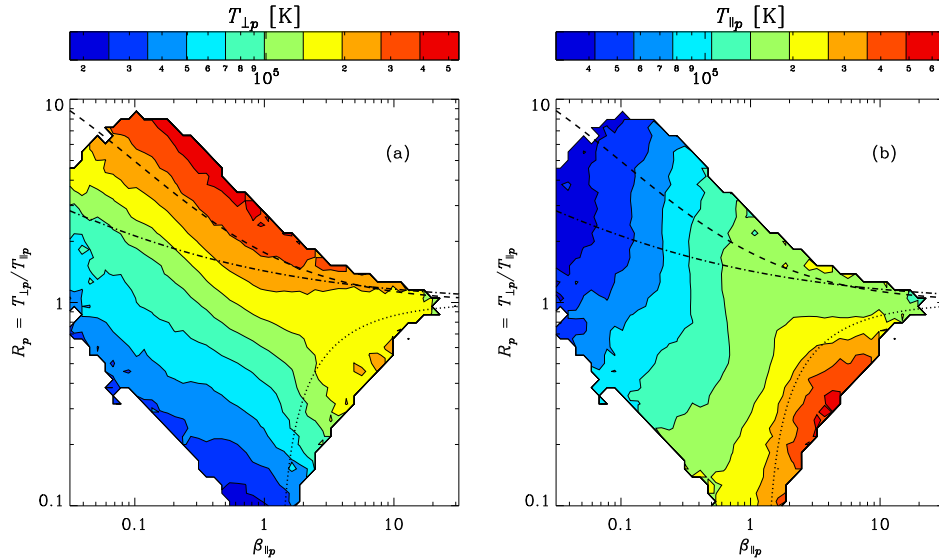


**Figure 4:** Plots of  $T_{\perp p}$  (a) and  $T_{\parallel p}$  (b) over the  $(\beta_{\parallel p}, R_p)$ -plane. The overlaid curves are thresholds for the oblique firehose (dotted), mirror (dashed), and cyclotron (dot-dashed) instabilities [Hellinger *et al.*, 2006]. The enhancements are mainly in  $T_{\perp p}$  for plasma beyond the mirror threshold and in  $T_{\parallel p}$  for plasma beyond the firehose threshold [Maruca *et al.*, 2012].

tons (color scale) as long as their differential speed (vertical axis) satisfies the threshold condition (two horizontal lines). **This demonstrates that ion-cyclotron resonance contributes to the heating of the corona/solar wind. This result was the topic of a March 2013 NASA Feature Story and was highlighted by the Physical Review letters as a featured article.** While this *Wind* result established that ion-cyclotron resonance is an active process in the heliosphere, *Solar Probe Plus* measurements will be necessary to determine its relative importance as a function of heliocentric distance. Thus, *Wind* has helped to frame one of the measurement objectives of *Solar Probe Plus*.

Another clue of the heating of the solar wind was obtained by Pulupa *et al.* [2013] by combining *Wind*/3DP electron measurements with *Wind*/WAVES thermal noise observations. Suprathermal electrons emitted by the solar corona travel significantly faster than the core solar wind proton population. To maintain current balance, the low-energy core component of the solar wind electrons has travel slower than the protons. Pulupa *et al.* [2013] were able to accurately derive the core electron flow speed after painstakingly reanalyzing the *Wind*/3DP electron data and properly accounting for a dipole term in the spacecraft potential (a feat not accomplished on other solar wind missions) and found a strong dependence on the collision age of the plasma parcel analyzed. Collisionally young parcels (with fewer collisions) show very large sunward electron drifts for the core electron component, while more collisional parcels show very similar electron flow speeds as for the protons (see Figure 3). **This result implies that collisions in the solar wind play an important role to eliminate the differential speed between**

**the electrons and protons resulting in solar wind heating.**

Studies using *Wind* have also recently found relationships between the total ion temperature and the anisotropy of the ion temperature,  $R_p \equiv T_{\perp p}/T_{\parallel p}$ , relative the instability thresholds for ion cyclotron, firehose, and/or mirror instabilities [e.g., Maruca *et al.*, 2011]. The studies found that the solar wind protons could get heated to some theoretical threshold anisotropy, then ion cyclotron, firehose, or mirror instabilities would get excited and act to reduce the anisotropy. These results (see Figure 4) provide evidence to suggest that instabilities can limit  $R_p$  in the solar wind. Further investigation showed that instabilities can affect the temperature anisotropy of  $\alpha$ -particles,  $R_\alpha$ , as well [Maruca *et al.*, 2012]. These results showed, for the first time, that even minor solar wind ions could potentially lead to the growth of instabilities near 1 AU. **The implications are that instabilities may be playing an active role in solar coronal heating and/or solar wind acceleration.**

Wilson III *et al.* [2013a] examined the effects of large amplitude ( $\delta B/B_o \sim 0.3$ ) high frequency ( $\omega/\Omega_{ce} \sim 0.2$ ) whistler mode waves on the electron distributions observed downstream of four supercritical interplanetary shocks. They found evidence to suggest that whistler waves were driven unstable by a heat flux instability and that they, in turn, caused a temperature anisotropy,  $(T_{\perp}/T_{\parallel}) > 1$ , for the halo electrons. They also found that the whistler wave amplitudes were correlated with the halo-to-core temperature ratio,  $T_{eh}/T_{ec}$ , and the normalized electron heat flux,  $|\bar{\mathbf{q}}_e|/q_o$  [see Figure 2 in Wilson III *et al.*, 2013a]. These results suggest that whistler mode waves help to regulate the electron heat flux in the solar wind and they may play

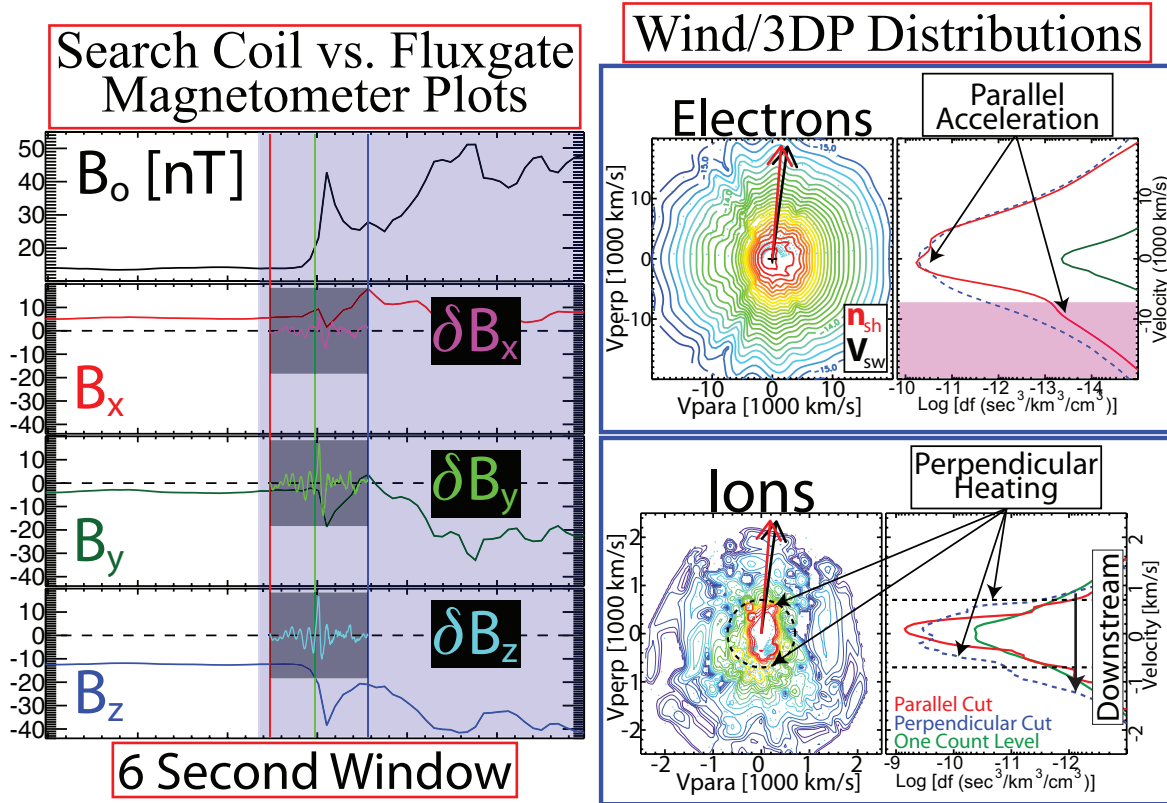


**Figure 5:** Example IP shock crossing observed by *Wind*. The fluxgate ( $B_o$  at  $\sim 11$  sps) and search coil ( $\delta B$  at  $\sim 1875$  sps) magnetometer data are plotted in the middle panels for a  $\sim 6$ s window around the shock ramp. The blue shaded region indicates the time over which the electron (top) and ion (bottom) particle distributions were sampled. The parallel electron acceleration and perpendicular ion heating observed simultaneously with the  $\sim 20$  nT wave illustrate the unique capacities of *Wind* [Wilson III et al., 2012].

an active role in the formation of the electron halo.

### Wave-Particle Interactions

Due to the collisionless nature of the solar wind plasma, the most efficient form of energy and momentum transfer is due to wave-particle interactions. *Wind* observed direct evidence of wave-particle interactions at collisionless IP shocks [Wilson III et al., 2010, 2012]. *Wind* is equipped with a waveform capture instrument called the Time Domain Sampler (TDS), part of the *Wind*/WAVES investigation. The TDS receiver is capable of fully resolving electric and magnetic fluctuations from  $\sim 3$  Hz up to  $\sim 60$  kHz. *Wind* can also examine full  $4\pi$  steradian electron and ion distributions with  $\sim 3$ s time resolution for the ions and a  $\sim 0.01$ s effective time resolution for the electrons [see Wilson III et al., 2012, for more details]. Both the *Wind* particle and wave measurements are unrivaled among solar wind missions.

Figure 5 shows an example of new results from *Wind* [results from Wilson III et al., 2012]. The observations provide evidence to support previous simulations [e.g., Cairns and McMillan, 2005] that found oblique electromagnetic waves could cause stochastic parallel – with respect to the quasi-static magnetic field – electron acceleration (potentially to relativistic energies) and perpendicular ion heating. **These results were high-**

**lighted on the NASA homepage news feed in July 2012 at Riding the Plasma Wave.**

Wave-particle studies using *Wind* have not been limited to the solar wind. Recent STEREO observations of very large amplitude whistler mode waves in the terrestrial radiation belts [Cattell et al., 2008] led to a number of similar studies with *Wind* [Kellogg et al., 2010, 2011; Kersten et al., 2011; Wilson III et al., 2011]. Unlike STEREO, *Wind* has the advantage of a search coil magnetometer and thermal particle distributions, allowing for a well defined determination of the wave propagation direction, magnetic field amplitude of the fluctuations, and instability threshold estimates. One wave was found to have  $\delta B \geq 8$  nT (peak-to-peak),  $\delta E \geq 300$  mV/m, and a lower bound on the Poynting flux of  $\gtrsim 300 \mu\text{W}/\text{m}^2$  [Wilson III et al., 2011], roughly 4 orders of magnitude larger than any previous observation. That single wave packet had enough energy density to energize plasma sheet electrons to  $\geq 1$  MeV, filling a  $3 R_E$  column with a flux of  $\sim 10^6 \text{ cm}^{-2} \text{ s}^{-1}$  in  $\sim 33$  seconds, assuming a  $\sim 1\%$  efficiency [see Santolík et al., 2010, for more details]. In addition, *Wind* also found conjunctions between these very large amplitude whistlers and electron microbursts observed by SAMPEX [Kersten et al., 2011]. These results influenced the design of and are currently influencing the studies

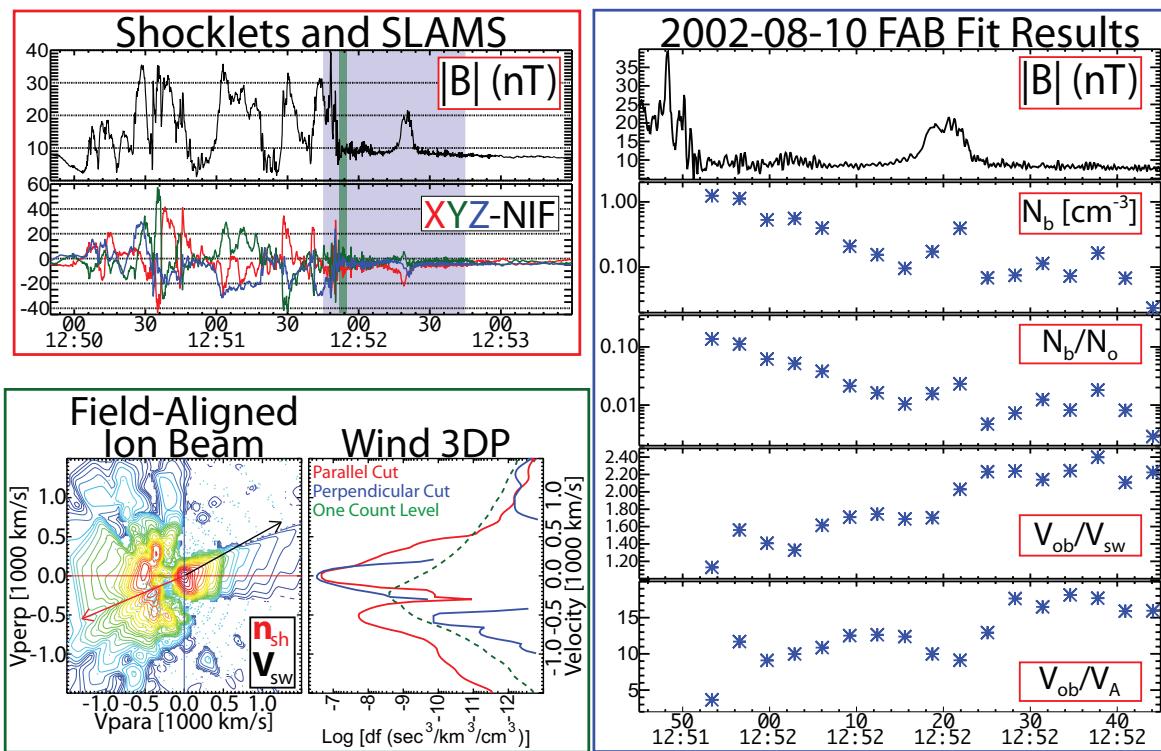


**Figure 6:** (upper left) Overview of the magnetic field profiles of a series of shocklets and SLAMS observed by *Wind*/MFI. The green and blue shaded regions corresponds to the time periods for the lower left-hand panel and the right-hand panel, respectively. (lower left) Ion velocity distribution showing contours of constant phase space density (bulk flow frame) in the plane containing  $B_o$  and  $V_{sw}$ , where  $B_o$  is along the horizontal. To the right are cuts of the distribution function, where the colors correspond to the red(parallel) and blue(perpendicular) crosshairs in the contour plot. (right panel) Results of fitting bi-Maxwellians to the FABs showing, in the following order,  $B_o$ ,  $n_b$ ,  $n_b/n_o$ ,  $V_{ob}/V_{sw}$ , and  $V_{ob}/V_A$  [Wilson III et al., 2013b].

performed by the *Van Allen Probes*.

### Particle Acceleration

Recently, *Wind* legacy observations were made in the terrestrial foreshock showing field-aligned ion beams (FABs) produced by short large amplitude magnetic structures (SLAMS) [Wilson III et al., 2013b]. **These results are important because they present a new way for ions to be accelerated without requiring something as large as the bow shock. Moreover, these results add evidence to support theories of diffusive shock acceleration (DSA),** whereby particles gain energy by traversing a shock ramp multiple times and diffuse in pitch-angle and energy by scattering off of upstream and downstream fluctuations. They argued that the FABs (see Figure 6, lower left-hand panel) were generated in a manner similar to those produced at the quasi-perpendicular bow shock. They also found that the solar wind core ions and electrons were strongly heated anisotropically within the group of SLAMS (see Figure 6, upper left-hand panel).

The FAB density (see Figure 6, right-hand panel) was found to decrease with increasing distance away from the upstream(sunward) edge of the group of SLAMS. A slight peak was found on the upstream(sunward) edge of the isolated SLAMS seen at  $\sim 12:52:20$  UT, with a quick decrease immediately after. They argued that

this showed that isolated SLAMS could reflect ions as well, but no where near as efficiently as groups of SLAMS.

These observations required high time, angular, and energy resolution ion measurements and high time resolution magnetometer data. The burst mode capabilities of *Wind* allowed for continuous coverage of low energy ( $\leq 30$  keV) particles through the entire group of SLAMS shown in Figure 6.

Shock-shock interaction is a well-established particle acceleration mechanism in astrophysical and space plasmas, but difficult to study observationally. Recently, the IP shock collision with the bow shock of the Earth on 1998 August 10 was identified as one of the rare events where detailed in-situ observations of the different acceleration phases can be made, due to the advantageous spacecraft and interplanetary magnetic field (IMF) configurations. The novel result of Hietala et al. [2011] was the first in-situ observations of the particle release at shock collision, further verified with a follow-up simulation study [Hietala et al., 2012].

Hietala et al. [2011] used energetic ion data from the ACE, *Wind*, and *Geotail* spacecraft. After crossing a tangential discontinuity (TD), the spacecraft moved into a flux tube that was connected to the IP shock and filled with a seed population of energetic particles. Since ACE was magnetically connected to the IP shock

but not to the bow shock, the seed population could be characterized by its measurements. ACE observations thus made it possible to distinguish the contribution of the bow shock and the shock-shock interaction to the particle acceleration.

*Wind* observed several particle bursts coming from the bow shock direction during the first part of the event (see Figure 7). These bursts corresponded to times when the spacecraft was connected to the quasi-perpendicular flank of the bow shock. Later, *Wind* became continuously connected to both shocks, and measured an increasing flux as well as two counter-streaming populations until the IP shock crossing.

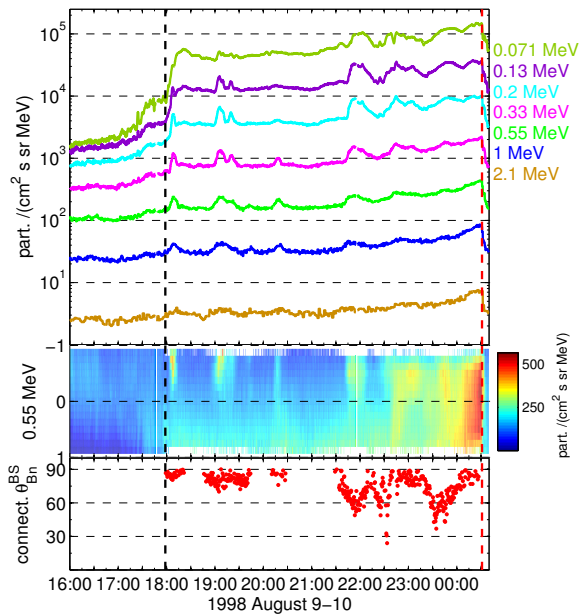


**Figure 7:** Energetic proton observations of *Wind* spacecraft. From top to bottom: the intensity of omnidirectional energetic particle flux in different energy channels, the pitch-angle cosine distribution in one energy channel, and the angle between the traced magnetic field line and the model bow shock normal at the connection point. The black dashed line shows the beginning of the radial IMF, and the red dashed line shows the IP shock passage. Adapted from *Hietala et al. [2011]*.

*Geotail* was located closest to the Earth and continuously connected to both shocks. It recorded the highest intensity at the IP shock crossing. Furthermore, immediately after the crossing *Geotail* observed a burst of very high energy particles propagating sunwards. Based on the velocity dispersion of the burst and the analysis of the geometry of the two shocks, *Hietala et al. [2011]* deduced that these particles had been released from the magnetic trap between the shocks as they collided.

*Hietala et al. [2012]* used a global 2.5D test-particle simulation to further study particle acceleration in this event. They concentrated on the last phases of the shock-shock interaction, when the shocks approach and pass through each other. The results of the simulation show a drop in the test-particle density after the shocks

pass through each other. The drop propagates downstream along the magnetic field lines at the speed of the last escaping particles. The arrival of this drop to *Geotail*'s location ends the increase in the test-particle density. Comparison of the simulation results with the observations of *Wind* and *Geotail* verified that the main features of the measurements can be explained by shock-shock interaction in this magnetic geometry, and are in agreement with the previous interpretation made by *Hietala et al. [2011]* of particle release.

### Turbulence and Intermittency

It has long been known that the small scale turbulent fluctuations in the solar wind do not have an equipartition of energy between the velocity and magnetic field fluctuations [e.g., *Belcher and Davis Jr., 1971*]. Early explanations for this were that pressure anisotropies were not accounted for in the normalization of the magnetic field, but recent theories suggest that this non-equipartition can be an inherent feature of MHD turbulence.

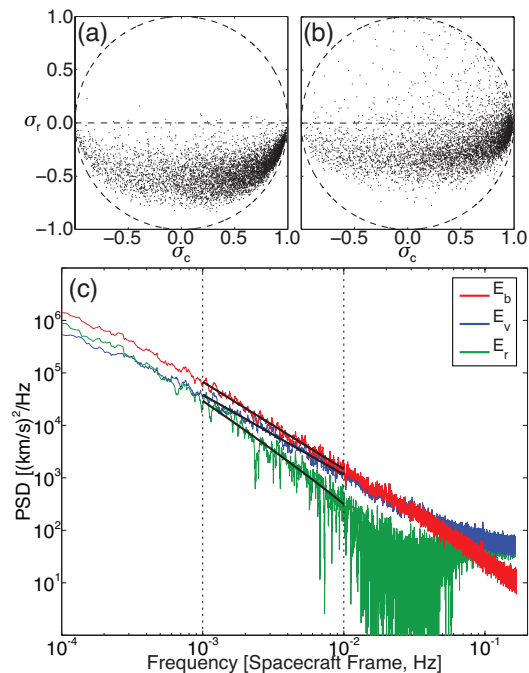


**Figure 8:** Distribution of residual energy  $\sigma_r$  and cross helicity  $\sigma_c$  with the standard normalization (a) and with the temperature anisotropy and drift corrections (b). The residual energy is closer to zero in the corrected normalization. (c) Power spectrum of magnetic field  $E_b$ , velocity  $E_v$ , and residual energy  $E_r$ . The residual energy spectrum (with spectral index  $\sim -1.9$ ) is steeper than the other spectra [*Chen et al., 2013*].

*Chen et al. [2013]* analyzed 5 years of *Wind* data, using MFI for the magnetic field fluctuations, 3DP for the velocity fluctuations and SWE for the temperature anisotropies and species drifts. They found that when correcting for the temperature anisotropies and drifts, the amount of non-equipartition is reduced, but there is still some “residual energy,” which has, on average, a spectrum with a power law of  $-1.9$  (see Figure 8). This

is remarkably close to the value found in recent MHD turbulence simulations [Boldyrev *et al.*, 2011].

The physical mechanism proposed in the theory is that residual energy is generated in modes with a parallel wavenumber of zero, which do not have to come to equipartition since they are zero frequency and therefore not waves [Boldyrev and Perez, 2009]. This condensate of residual energy, generated by the turbulent dynamics, then interacts non-locally with the cascade causing the non-equipartition. The results of Chen *et al.* [2013] show that this is a plausible mechanism to explain this long standing mystery of solar wind physics.

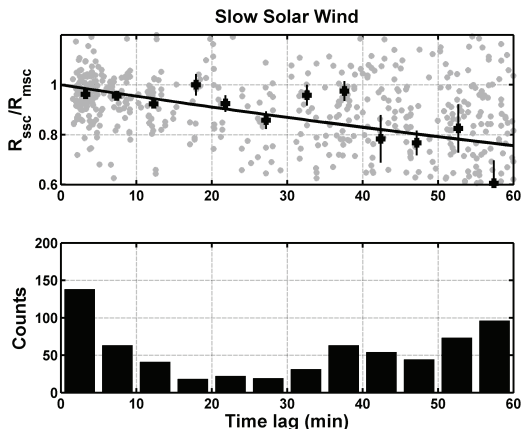


**Figure 9:** The top panel shows Eulerian correlation values ( $R_{ssc}/R_{rmsc}$  plotted in gray dots) determined from magnetic field data, the mean Eulerian correlation values for 6 minute wide bins, and the black curve shows the Eulerian correlation function for the slow solar wind ( $V_{sw} \leq 450$  km/s) as a function of time lag. The bottom panel displays the number of Eulerian correlation data points that went into each mean. The Eulerian correlation function gives the rate of de-correlation in the plasma frame [Weygand *et al.*, 2013].

The de-correlation of the magnetic field fluctuations is the principal contributor to the violation of the frozen-in assumption and a fundamental property of turbulence dynamics. Understanding this de-correlation will provide important insights into plasma turbulence theory. To produce Figure 9, Weygand *et al.* [2013] identified thousands of slow solar wind intervals with simultaneous data from pairs of spacecraft lasting 12 hours, with little to no large rotations in the IMF  $B_x$  and  $B_y$ , and little to no large gradients in the total magnetic field, flow, and density. The magnetic field data and plasma data were obtained from various pairs of the ACE, *Geotail*, *Interball*, THEMIS B and C, and *Wind* spacecraft. These spacecraft pairs covered spatial separation from about  $10 R_E$  up to about  $240 R_E$ . From each interval they were able to get a cross correlation of the magnetic field vectors between the spacecraft pairs as well as an equivalent autocorrelation value of the magnetic field, which was determined using a lag time obtained from the mean spacecraft separation and the mean solar wind speed for the interval considered.

The values used in the top panel of Figure 9 are those pairs that consist of just spacecraft where the spacecraft separation vector is within 30 degrees of the solar wind flow vector to ensure that both spacecraft measures the same parcel of solar wind. Finally the de-correlation time is obtained from an exponential fit (decay time) to the mean values in Figure 9 and was determined to be  $215 \pm 43$  min in the slow solar wind. Similar results were produced for the fast solar wind ( $V_{sw} > 500$  km/s) and the de-correlation time was determined to be  $114 \pm 23$  min. This difference is most likely due to the different characteristics of the turbulent magnetic field fluctuations (i.e., quasi-two-dimensional turbulence versus slab like turbulence) in the slow and fast solar wind.

The Eulerian correlation functions have important implications for understanding solar wind turbulence and making space weather predictions. Time de-correlation imposes limits to space weather prediction, it is responsible for departures from the frozen-in flow condition, and it also influences cosmic ray particle scattering in several important ways. This study could not have been done without simultaneous pairs of spacecraft within the solar wind for extended periods of time over a wide range of spatial separations.

### 2.1.2 Magnetic Reconnection

Magnetic reconnection is a very rapid process by which magnetic field energy is directly transferred to particles. In order to study this process in the solar wind, extremely high cadence plasma and magnetic field measurements are required, such that only *Wind* can provide. Farrugia *et al.* [2012] described a  $\sim 4$  hour-long solar wind transient observed by the *Wind* spacecraft, in which a pressure-balanced structure is embedded. Minimum variance analysis on high resolution ( $\sim 11$  sps) magnetic field data shows it to be planar to an excellent approximation (ratio of intermediate-to-minimum eigenvalues  $\sim 83$ ). The structure starts with a very sharp discontinuity whose orientation coincides within four degrees with that of the structure itself. They found that this discontinuity has a bifurcated magnetic field and plasma flow structure. There is also a velocity depression coextensive with it. Applying a tangential stress balance test – Walén relation – to the discontinuity, they found a good agreement between predictions and observations. They directly show the presence of two Alfvén waves propagating in opposite directions. The observation is consistent with the presence of a reconnection region in a hitherto unexplored configuration within a small solar wind transient.

The association between electron phase space holes (EHs) and current sheets observed by *Wind* (see Figure 10) demonstrates the presence of active streaming instabilities at solar wind current sheets. Specifically, the data strongly suggest an electron two-stream instability driven by magnetic reconnection. Mounting

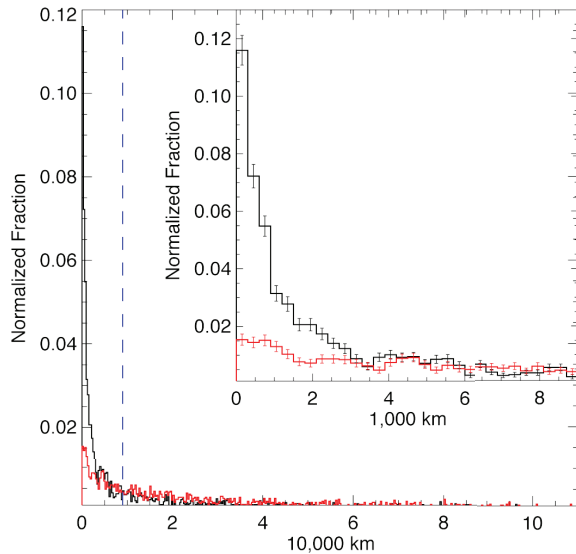


**Figure 10:** Distributions (normalized to 1) of distances between *Wind* and the closest current sheet for: ESW observation times (black trace) and randomly chosen observation times (red trace). Inset plot shows a close up of short distances, indicated by the dashed line in the primary plot [Malaspina et al., 2013a].

evidence from turbulence observations and simulations [e.g., Daughton et al., 2011; Osman et al., 2012] as well as observations and simulations of magnetic reconnection in the solar wind [e.g., Drake et al., 2003; Gosling, 2007] suggest that the majority of energy transfer from magnetic field configurations to the heating and acceleration of solar wind plasma occurs at localized current sheets. The study by Malaspina et al. [2013a] not only supports the idea of the transfer from magnetic energy to particle energy at localized current sheets, it identifies one of the active instabilities as electron two-stream.

*Wind* is unique in that it is the only solar wind mission where the observational association between EHS and current sheets could have been established, due to its unique combination of high-quality high-cadence magnetometer, electric field waveform, and particle data.

### 2.1.3 Summary and Relevance

The new re-calibrated *Wind*/SWE measurements [e.g., Kasper et al., 2013; Maruca et al., 2012] have led to a re-examination of the temperature evolution of the solar wind and the instabilities which dominate. These results, combined with a re-examination of the *Wind*/3DP electron measurements **have fundamentally changed our understanding of the evolution of the solar wind from the Sun to the Earth and provided essential measurement constraints for future missions like *Solar Probe Plus*.**

The results from Wilson III et al. [2012] have important implications because they **show the first direct evidence of a mechanism that can produce**

**suprathermal particles from the thermal core, which may help to resolve the “injection problem.”** Moreover, the same wave-driven electron acceleration mechanism has been proposed to explain solar flare electron energization. The results from the terrestrial radiation belts [e.g., Kellogg et al., 2010; Kersten et al., 2011; Wilson III et al., 2011] have led to multiple questions currently being investigated by the *Van Allen Probes* (RBSP). **The extreme energy fluxes of these large amplitude whistler mode waves in the radiation belts may have implications that fundamentally change our understanding of radiation belt dynamics.**

The results from Wilson III et al. [2013b] are important because they **present a new way for ions to be accelerated without requiring something as large as the bow shock. Moreover, these results add evidence to support theories of diffusive shock acceleration (DSA),** whereby particles gain energy by traversing a shock ramp multiple times and diffuse in pitch-angle and energy by scattering off of upstream and downstream fluctuations.

The results from Hietala et al. [2011, 2012] **show that shock-shock interactions are capable of enhancing particle energization in collisionless shocks by increasing the energy of the affected particles by 2–3 times that produced by the IP shock alone.** It is important to note that *Wind* has the capacity to observe the entire  $4\pi$  sky for these energies, which is unique for L1 monitors.

Finally, the unique capabilities of *Wind* have allowed studies to significantly improve our understanding of the fundamental processes involved in solar wind turbulence and magnetic reconnection.

## 2.2 Heliophysics Objective #2

The second heliospheric research objective, as described by the *Science Plan for NASA’s Science Mission Directorate 2007-2016*, focuses on how the heliospheric manifestations of solar activity evolve before reaching Earth and how they affect the magnetosphere. The Sun’s output varies on many time scales. *Wind*’s high time resolution, stable and reliable measurements carried out over 18 years (nearly two solar cycles) have significantly contributed to studies of solar wind structures on all scale-lengths ranging from turbulent energy cascade to the structure and propagation of ICMEs. This section highlights some of the outstanding *Wind* results from this area.

### 2.2.1 Evolution of ICMEs: Inner Heliosphere Evolution of Cross-Section

The investigation of the ICME evolution in the inner heliosphere has been undertaken from two, quite separate, points of view: remote sensing and in-situ observations. In the recent years, the availability of heliospheric imaging has provided the impetus to link the

events from these two perspectives. The flattening and distortion of the ICME structure in the remote sensing observations has been touted as evidence of pancaking. Meaning, the consequence of the ICME interaction with the ambient solar wind as the ICME plows into the slower moving solar wind ahead of it. Yet analytical models used to reconstruct the local geometry of the event that rely on the in-situ single point time-series magnetic field data taken by spacecraft as they fly through the structure, show good agreement with a simple circular cross-section. Though most models assume a force-free condition and thus result in circular cross-section flux rope structures, a number of recent studies [e.g., *Nieves-Chinchilla et al.*, 2011] have successfully relaxed this assumption and attempted to account for the plasma pressure inside the ICME. Yet, these new models still show a very minor deviation from a circular cross-section (see Figure 11).

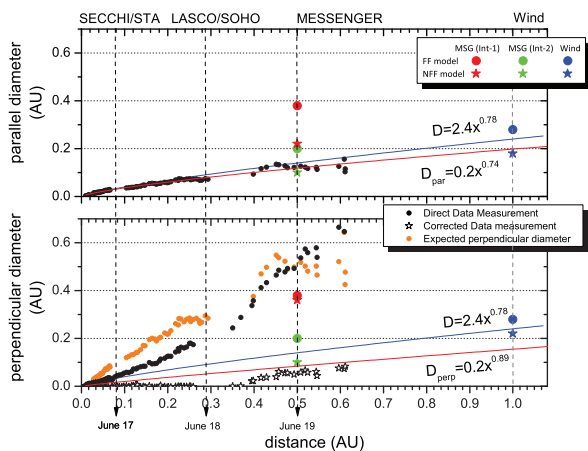


**Figure 11:** Combined analysis of the expansion of the parallel (top) and perpendicular (bottom) diameters (corrected) of the ICME/CME cross section over 1 AU. The dots/stars represent measurements from SECCHI images (black), analytical model results for 0.5 and 1 AU (green, red, and blue), and expected perpendicular diameters (orange). The blue lines are the empirically derived expansion of a circular cross section. The red line represents the fit to the deprojected perpendicular data from  $\sim 0-0.3$  AU [Figure 10 from *Nieves-Chinchilla et al.*, 2012].

Combining *Wind* and MESSENGER inner heliospheric in-situ measurements of the June 16-20, 2010 ICME with white light observations from both STEREO spacecraft and from SOHO, *Nieves-Chinchilla et al.* [2012] have shown that the “pancaking” distortions are likely projection effects and the near circular cross-section model results from in-situ data (mostly from *Wind*) are more reliable. This significant result will influence the development of global heliospheric models that also show significant “pancaking” [e.g., *Riley and Crooker*, 2004; *Riley et al.*, 2004] though they do not include the significant magnetic pressure of ICMEs. Most recently, *Savani et al.* [2011], has developed a semi-empirical model of ICME expansion that asymptotes a fixed aspect ratio for the cross section, in agreement with the *Wind* observations.

## Global Geometry

While substantial progress has been made in determining the cross-sectional geometry of flux rope type ICMEs, little is known of their third dimension near 1 AU. Coronagraph images of young ICMEs show a familiar horse-shoe shaped structure, however multi-point in-situ observations rarely find that this simple geometry is preserved further out in the heliosphere. *Kahler et al.* [2011] have used *Wind* energetic electrons and magnetic field observations within a number of ICME to constrain the global geometry. Using *Wind*/3DP energetic electron burst dispersion, they could compute the total distance these particles traveled along the ICME field lines, assuming they all started at identified Type III radio burst observed by *Wind*/WAVES. Thus, the obtained field line lengths could be compared to a fitted magnetic flux rope yielding very good agreement deep inside the flux rope, but significant deviations near the ICME boundaries. **This *Wind* result implies that ICMEs continually interact with their magnetic environment likely via magnetic reconnection resulting in changing size and orientation.**

Moreover, counter-streaming heat flux electrons usually observed inside ICMEs would imply that both foot points of the ICME are still magnetically connected to the Sun. However, recently *Reames et al.* [2009] have used *Wind* energetic particle observations to identify  $\sim 4-20$  MeV/nucleon ions inside magnetic clouds with abundancies of He, C, and O that clearly show them to be “anomalous” cosmic rays (ACRs) that are known to be accelerated in the outer heliosphere. Thus during the 3-4 days that these ICMEs needed to expand to 1 AU they have been somehow filled with ACRs implying some sort of magnetic connection to open field lines. Understanding the simultaneous observation of ACRs and bidirectional electrons in magnetic clouds has been a challenge to our understanding of the magnetic topology of ICMEs and the mechanism of cross-field particle transport that is normally observed to occur only on a much longer time-scale [*Reames*, 2010, 2013].

## Rotation and Non-Radial Propagation

Besides the expansion and distortion of the ICME cross section, ICMEs have been observed to rotate or twist as a whole as they propagate outward from the Sun [e.g., *Vourlidis et al.*, 2011]. However, this global evolution was not captured by in-situ spacecraft till the MESSENGER/*Wind* analysis of *Nieves-Chinchilla et al.* [2012]. They have shown that while the June 16-20, 2010 ICME was rotating significantly in the field of view of white light coronagraphs, this trend continued from 0.3 to 1.0 AU. **This discovery has a significant implication on the accuracy of space weather predictions, namely that ICMEs cannot be simply ballistically propagated from their coronal origin to 1 AU, but their interactions in the in-**

ner heliosphere has to be considered [See Figure 6b from *Nieves-Chinchilla et al.*, 2012].

Another *Wind* measurement that was widely and successfully used to determine ICME propagation properties in the inner heliosphere is the Type II radio bursts observed by the *Wind*/WAVES instrument. *Xie et al.* [2012] successfully combined STEREO and SOHO white light observations with these *Wind* radio measurements, along with 1 AU in-situ parameters and ENLIL model results to show that for the April 3, 2010 ICME the Earth arrival time of the driven shock can be predicted to within a few hours. While *Vasanth and Umamathy* [2013] argue that faster and larger Earth-bound ICMEs tend to have clear Type II radio signatures in the *Wind*/WAVES data, *Gopalswamy et al.* [2012] identified 21 radio-loud ICMEs from Sun disk center that had no in-situ shock counterparts at Earth. They argue that, just as *Nieves-Chinchilla et al.* [2012] found, that these ICMEs were weaker and hence could be easily deflected from pure radial propagation, and thus missed Earth all together. **These results all illustrate the promise of combining remote sensing white light and radio observations with in-situ plasma measurements to determine the inner heliospheric propagation and evolution of ICMEs.**

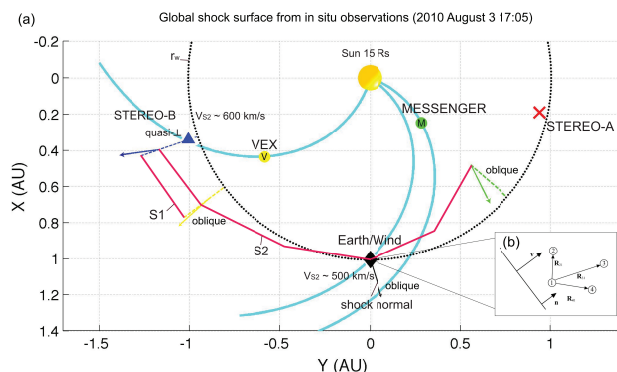


**Figure 12:** (a) Global configuration of two shock fronts S1 and S2, estimated at the time of the shock observation at *Wind* (2010 August 3 17:05 UT). The approximate shape of the shocks (red solid lines) is shown by estimating the heliocentric distance of the shocks at each location for the given point in time. For S2, shock normals are drawn as arrows in the color consistent with the spacecraft position, the configuration of the shock is indicated as oblique or quasi-perpendicular. The nominal Parker spiral field is drawn connecting the Sun to each spacecraft for the upstream conditions of solar wind speed 450 km/s at STEREO-B and VEX and 400 km/s at *Wind* and MESSENGER. Note that VEX and STEREO-B are approximately connected by the nominal Parker spiral eld. (b) The insert shows an illustration of the 4-spacecraft method to determine the shock normal orientation near Earth, using *Wind*, ACE and ARTEMIS. A planar shock is measured at 4 points in space for which the distances to one reference spacecraft have to be known.

### ICME-ICME Interactions

Aside for the ambient solar wind affecting the propagation and deformation of ICMEs, during solar max-

imum years these geo-effective structures also interact with each other. Recently, *Möstl et al.* [2012] analyzed a number of interacting ICMEs departing the Sun on August 1, 2010. They have employed SDO, SOHO and STEREO for white light observations and MESSENGER (at 0.38 AU), VEX (at 0.72 AU) and *Wind*, ACE, ARTEMIS and STEREO-B near 1 AU. The magnetic flux rope configuration and the driven shocks were individually fitted at each spacecraft and indicate that while the ICMEs were interacting with each other, they have not completely merged by 1 AU (see Figure 12). VEX and STEREO-B observed similar magnetic flux ropes, in contrast to structures at *Wind*. MESSENGER received a glancing blow of the ICMEs, and the vents completely missed STEREO-A.

These observations demonstrate how sympathetic solar eruptions may immerse at least a third of the heliosphere in the ecliptic with their distinct plasma and magnetic field signatures. They also emphasize the difficulties in linking the local views derived from single-spacecraft observations to a consistent global picture, pointing to possible alterations from the classical picture of ICMEs. **The multi-point, in-situ observations of a complex sequence of coronal mass ejections, presented by *Möstl et al.* [2012] and in that of *Harrison et al.* [2012] may serve as a benchmark event for numerical and empirical space weather prediction models.**

### 2.2.2 CIRs and Particle Acceleration

Corotating Interaction Regions (CIRs) form when a stream of fast solar wind overtakes a parcel of slow solar wind that was emitted from the Sun at an earlier time. This interaction creates a compression region that corotates with the Sun and can strengthen to form shocks that accelerate particles. CIRs are the primary producer of the tens of keV to several MeV/nucleon energetic particles measured at 1 AU during periods of low solar activity.

The common interpretation is that these enhancements arise from the sunward propagation of particles accelerated at CIR-driven shocks between  $\sim 2$  to 5 AU; these particles lose energy and are scattered as they travel inward against the outward flowing solar wind resulting in a turnover in their energy spectrum below  $\sim 0.5$  MeV/nucleon [see *Fisk and Lee*, 1980]. This interpretation has accounted for a number of CIR particle event features, including the large intensity gradients in the inner heliosphere and the exponentially decaying spectral profiles, the primary exception being the spectral profiles at 1 AU where the predicted turnover at lower energies is generally not seen [see review by *Richardson*, 2004]. Recent studies have shown that these lower energy, or suprathermal, CIR-associated particles can be accelerated at 1 AU in CIRs with a reverse shock or a well-formed compression region trail-

ing edge [e.g., *Ebert et al.*, 2012a].

*Ebert et al.* [2012b] investigated this topic by examining the first-order flow anisotropies of  $\sim 0.06$ - $0.95$  MeV/nucleon He ions during three CIR associated He intensity enhancements observed at 1 AU by *Wind*. They studied an event with (1) a reverse shock, (2) a well-formed compression region, and (3) a weak compression region. The anisotropies were calculated using 20 minute averaged He intensity observations from EPACT/STEP, 20 minute averaged interplanetary magnetic field observations from the magnetic field investigation, and 20 minute averaged plasma velocity observations from the SWE. The He ion anisotropies in the events with a reverse shock and well-formed compression transitioned from anti-sunward to sunward as the compression region trailing edge moved over the spacecraft (Figure 13), suggesting that the trailing edge was organizing the flows and was a local source for the particles. The event with the weak compression had predominantly sunward flows throughout, indicating that the source of the He ions was beyond 1 AU.

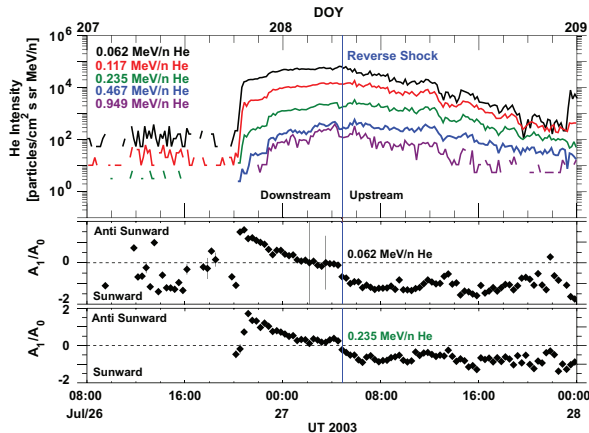


**Figure 13:** CIR-associated He ion enhancement from July 26–28, 2007, identified by *Wind* EPACT/STEP. Shown (from top to bottom) are 10 minute averaged 0.062–0.949 MeV/nucleon He intensities, and 20 minute averaged first-order anisotropies ( $A_1/A_0$ ) at 0.062 and 0.235 MeV/nucleon He, respectively. The He ion flow transition, from anti-sunward to sunward, across the shock at the CIR trailing edge suggests that this boundary may be a local source for the particles.

These observations provided crucial information regarding particle transport in these events, allowing for further demonstration that CIR-associated He ions at 1 AU can be accelerate to suprathermal energies at the CIR trailing edge in events where the compression region is well formed. **These *Wind*-based anisotropy observations can also provide critical information for understanding particle transport in CME-driven energetic storm particle and solar energetic particle events, the type of transient events that will be frequently observed at 1 AU during the upcoming solar maximum period of solar cycle 24.**

### 2.2.3 Interplanetary Shocks: Inner Heliosphere

Besides ICMEs, IP shocks also have significant geo-effectiveness. They accelerate energetic particles event at 1 AU and compress the Earth’s magnetosphere resulting in sudden commencements. Traditionally, IP shocks are treated as simple planar structures when reaching Earth. To systematically estimate the shock front deviation from planarity on different scales, 62 IP shocks observed by *Wind* and at least one other spacecraft in the solar wind have been analyzed [*Koval and Szabo*, 2010].

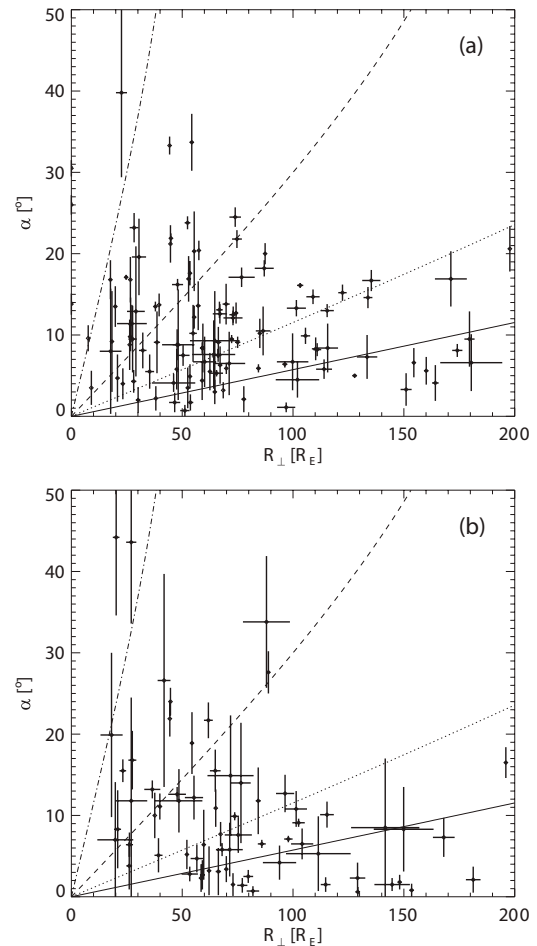


**Figure 14:** Normal difference between *Wind* and other spacecraft calculated using (a) *Wind* 3DP and (b) SWE data as a function of distance perpendicular to the *Wind* local shock normal. Solid, dotted, dashed, and dot-dashed lines indicate the model normal differences corresponding to shock curvatures of 1000, 500, 200, and 50  $R_E$ , respectively [*Koval and Szabo*, 2010].

The technique uses the local shock normal and speed calculated from the *Wind* measurements together with the times and locations of the shock observations by *Wind* and another spacecraft. It calculates, under the assumption of constant shock curvature on the scale of inter-spacecraft separation, the radius of curvature (i.e., the angle between the normal at the two locations on the shock surface).

Figure 14 shows the angle between the normals at two

locations on the shock surface calculated separately using the *Wind*/3DP (a) and SWE (b) data as a function of distance perpendicular to the *Wind* local shock normal. The results show the presence of local (on scales up to  $\sim 30 R_E$ ) shock curvatures with radii of less than  $\sim 50$  to  $\sim 200 R_E$  for the majority of analyzed shocks. On larger scales (greater than  $\sim 100 R_E$ ), the shock curvature decreases and reaches the limit of the strongest possible curvature with radius of  $\sim 400 R_E$  for all analyzed shocks. **This result implies that while IP shocks have a clear global curvature, they have, in addition, a corrugated surface.**

*Pulupa et al.* [2010] used *Wind* to examine the properties of 178 IP shocks comparing various parameters to the observation of upstream Langmuir waves. They found that the best predictor of enhanced wave activity was the de Hoffmann-Teller speed. This result is consistent with the theory that electrons are accelerated through a process known as the fast Fermi model (called “fast” because the energization occurs after a single encounter) [e.g., *Wu*, 1984]. They observed enhanced wave activity upstream of 43/178 shocks and that this activity occurs upstream of both quasi-parallel and quasi-perpendicular shocks. Other predictors of upstream wave activity were the upstream plasma density, upstream shock speed, and the downstream magnetic field magnitude.

In a follow-on study using *Wind*, *Pulupa et al.* [2011] found an asymmetry in Langmuir wave activity in the electron foreshock of the terrestrial bow shock. They found enhanced wave activity on the sunward side of the electron foreshock due to the reflection of strahl electrons coming from the sun. Since these beam-like electrons can only “see” the sunward side of the bow shock, if they are reflected, it will be back upstream on the sunward side [see Figure 2 in *Pulupa et al.*, 2011]. Therefore, they concluded that the asymmetry in the wave activity is due to a reflection of the electron strahl causing beam-driven Langmuir waves.

#### 2.2.4 Long-Term Variations

The long-term (18 years) of continuous solar wind observations of *Wind* were critical in compiling a catalogue of ICME, IP Shock, Corotating Interaction Region (CIR) and Stream Interaction Region (SIR) covering 1995 to 2011 [*Jian et al.*, 2012]. This catalogue also contains STEREO and ACE observations. *Jian et al.* [Figures 2 and 3, 2012] show the obtained ICME and SIR properties over more than a solar cycle. In contrast to the rising phase of solar cycle 23, the recurrent rate of stream interaction regions (SIRs), represented by the ratio of corotating interaction region (CIR) count to SIR count, in this rising phase is higher, probably because of the quieter Sun and fewer transients. SIRs have weaker maximum field and total pressure. After a slow start, the ICME occurrence rate finally increased

in 2011 and reached the level between 1999 and 2000, but ICMEs in this rising phase are generally smaller, weaker, and less expansive than in the last rising phase. During this rising phase, the ICMEs drive shocks less often and have weaker maximum field, consistent with the overall weaker IMF. All of the above features are manifestation of a weak cycle 24 in the solar wind.

*Richardson and Cane* [2010] also compiled a catalogue of near-Earth ICMEs using measurements from a number of spacecraft, including *Wind*. This catalog, extending from 1996 to 2009 and including details of the  $\sim 340$  ICMEs and their solar counterparts that were observed during this period, has been cited by 58 published papers. The catalog continues to be updated into solar cycle 24, and has been circulated via the web and by request to the authors. Specific *Wind* products that have been used to compile the catalog include MFI magnetic field, SWE and 3DP plasma data, the *Wind* shock list developed by J.C. Kasper and colleagues, and the *Wind* magnetic cloud list of R. Lepping and co-workers. The OMNI near-Earth solar wind database, which includes parameters observed by *Wind*, was also used. The catalog has been used to investigate the depressions of cosmic ray intensity due to these ICMEs [*Richardson and Cane*, 2011a] and studies of ICME geo-effectiveness as a function of speed [*Richardson and Cane*, 2011b]. The latter study may provide a statistical estimate of the geomagnetic activity that an approaching ICME viewed by a heliospheric imager might produce.

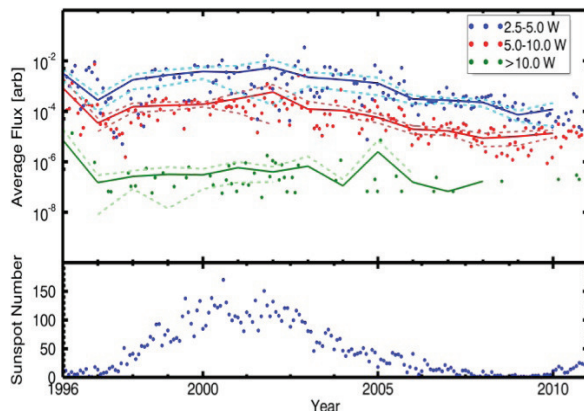


**Figure 15:** Long term average of suprathermal flux of He<sup>2+</sup> from 1996-2011. Top panel shows the flux from the STICS instrument in three distinct energy bins. The bottom panel shows the sunspot number [*Gruesbeck et al.*, 2012].

*Wind*/STICS is a time-of-flight mass spectrometer, therefore, it can differentiate many minor ionic species and look at their characteristics in the suprathermal energy range. By investigating these minor ionic species, the origin of the suprathermal plasma may be better understood. ***Wind* offers a unique ability to investigate the evolution of the suprathermal plasma and its reaction to the changing solar environment, as it has been collecting data since 1994 spanning multiple solar cycles.** Observing the evo-

lution of the suprathermal plasma aids our understanding of the acceleration and origin of these particles.

Recently, [Gruesbeck *et al.*, 2012] have analyzed the long-term evolution of suprathermal flux of H<sup>+</sup>, He<sup>2+</sup>, and other heavy ion species over the mission duration. The flux is separated into velocity bins of 2.5–5 V<sub>sw</sub>, 5–10 V<sub>sw</sub>, and > 10 V<sub>sw</sub>, effectively separating the flux into “low,” “high,” and “very high” energy bins. Additionally, the flux is accumulated using a dynamic cadence length determined by the number of non-zero measurements accumulated. Due to the unique orbit of *Wind* care was taken to omit time periods when the spacecraft was in the magnetosphere or near the bow shock. These periods were determined by the bow shock crossing list from the MFI team.

Figure 15 shows one such result of this analysis. It shows that the suprathermal flux does evolve slightly with the solar cycle. With the strongest modulation occurring for the lower energies. If SIR shocks were to be a strong influence on the suprathermal flux one would expect an inverse relationship, as there are more SIR shocks present during solar minimum. Shocks are known to be a primary source of acceleration for energetic particles such as solar energetic particles and anomalous cosmic rays. Recent studies have begun to look at the role of shocks in the acceleration of suprathermal particles. **However, an analysis of the suprathermal flux over the *Wind* mission show that SIR shock may not be an efficient accelerator of suprathermal particles at 1 AU.**

### 2.3 Heliophysics Objective #3

The third and final heliophysics research objective of the *Science Plan for NASA’s Science Mission Directorate 2007-2016* concerns safeguarding the journey of exploration. To maximize the safety and productivity of human and robotic explorers, scientists must establish the geomagnetic impact of solar activity (as manifested in the 1 AU solar wind) to the point that the development of accurate forecasting capabilities becomes a possibility. *Wind* served as an upstream solar wind monitor or as the primary observation post (during its magnetotail crossing phase) for the studies summarized next. This objective also benefits from the ICME and shock studies described in the previous section.

#### 2.3.1 Electron Variations

**Suprathermal electron populations, uniquely measured by *Wind*/3DP, carry important information about solar wind and energetic particle acceleration.** Wang *et al.* [2012] combined STEREO A and *Wind* observations finding that during 2007 March through 2009 March at solar minimum, the observed quiet-time superhalo electrons have a nearly isotropic angular distribution and a power-law spectrum (see Figure 16),  $f \propto V^{-\gamma}$ , with  $\gamma$  ranging from 5 to 8.7, with nearly half between 6.5 and 7.5, and an average index

of  $6.69 \pm 0.90$ . The integrated density of quiet-time superhalo electrons ranges from  $10^{-8} \text{ cm}^{-3}$  to  $10^{-6} \text{ cm}^{-3}$ , about  $10^{-9}$ – $10^{-6}$  of the solar wind density, and it, as well as the power-law spectrum, shows no correlation with solar wind protons.

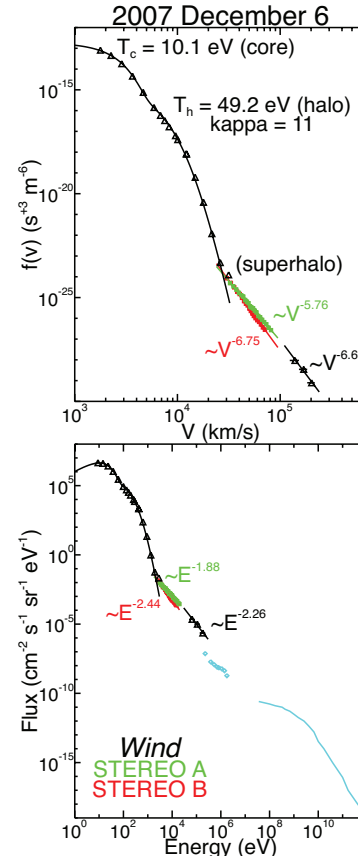


**Figure 16:** Quiet-time solar wind electron velocity distribution function spectra (top) and flux spectra (bottom) from  $\sim 9$  eV to  $\sim 200$  keV measured by *Wind* (black) and STEREO A (green) and STEREO B (red) on 2007 December 6. The solid lines represent the fit by a sum of a Maxwellian and a Kappa to the solar wind core and halo distribution and the power-law fit to the superhalo [Wang *et al.*, 2012].

The density of superhalo electrons decreases by approximately one order of magnitude between early 2007 and early 2009, probably reflecting the decay of solar cycle 23 and the approach to its unusually deep minimum activity, while the power-law spectral index  $\gamma$  has no solar-cycle variation. These quiet-time superhalo electrons are present even in the absence of any solar activity, e.g., active regions, flares or micro-flares, type III radio bursts, etc., suggesting that they may be accelerated by resonant waveparticle interactions in the interplanetary medium, or by nonthermal processes related to the acceleration of the solar wind such as nano-flares.

#### 2.3.2 Solar Energetic Particles

Large, gradual SEP events are generally recognized as due to particle acceleration by shocks driven by fast coronal mass ejections. This phenomena is of great in-

terest and has multiple applications and consequences.

### Timing SEP Acceleration Onsets

Particles from large SEP events arrive in inverse velocity order, i.e. the fastest particles arrive first as shown in the left panel of Figure 17. If one plots the onset time of each energy interval as a function of the inverse of the corresponding velocity,  $V^{-1}$ , then one finds the linear behavior shown in the right panel of Figure 17. Since time = distance/velocity, the slope of the fit line is the path length from the source to the observer and the intercept is the solar particle release (SPR) time of the particles. This technique has been used to derive SPR times for 30 large “ground-level events” (GLEs) where high-energy (GeV) protons cause a nuclear cascade through the Earth’s atmosphere to be seen at ground level [Reames, 2009a,b].

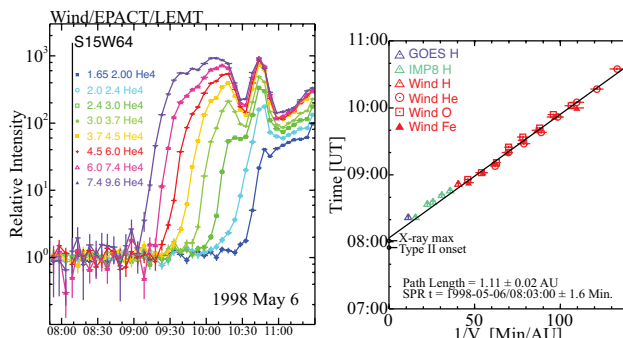


**Figure 17:** The left panel shows the relative intensity of  ${}^4\text{He}^{2+}$  as a function of time for May 6, 1998. The right panel shows the time from SEP acceleration versus  $V^{-1}$ .

The timing of these large events shows that acceleration does not begin until the CME-driven shock wave has propagated out to 2–3 solar radii. In many cases SPR times occur up to  $\sim 30$  min or more after the associated solar flare. The same technique has been used to study the SEP onset timing in conjunction with STEREO observations of the location CME and shock [Rouillard *et al.*, 2012]. **Beginning with recent events (e.g., 2012 May 17) it has been possible to combine *Wind* data with GeV proton data from Pamela as well as STEREO and SOHO observations of the CME and shock. Thus, begins a new era in the study of high-energy SEP acceleration near the Sun.**

### The Streaming Limit

In the early phase of extremely large SEP events, protons streaming out from the shock amplify resonant Alfvén waves in the interplanetary medium ahead of the shock. As the proton intensity increases the wave growth increases and particle scattering increases so that the increase in streaming begins to slow. Eventually the SEP intensities reach a limiting plateau value called the streaming limit. Recent studies of the particle energy spectra on this plateau using data from *Wind* and ACE have shown for the first time that spectra roll downward at low energies [Reames and

Ng, 2010]. The rollover is caused when higher energy protons scatter to larger pitch angles where they generate waves that can scatter low-energy particles with small pitch angles that are just beginning to arrive. This pitch-angle coupling is also important during the first few minutes of shock acceleration near the Sun (Ng and Reames 2008).

### SEP Acceleration at IP Shocks

Historically there has been a puzzle as to why some interplanetary shocks easily accelerate particles while others do not. What shock parameters control this acceleration? Recently, Reames [2012] studied in-situ acceleration of  $\sim 1$ –10 MeV/amu ions at 285 interplanetary shock waves observed by the *Wind* spacecraft. The most significant factor in acceleration was the shock speed; particle intensities increase strongly with shock speed. High shock compression ratio was also a factor as was  $\theta_{Bn}$ , the angle between the upstream magnetic field and the shock normal. Quasi-perpendicular shocks were favored, contrary to some recent theoretical predictions. The relationship of the particle spectral index to the shock compression ratio and the background spectral index was studied in detail and the importance of spectral “knees” was considered.

### SEP Angular Distributions

***Wind*, with its spin axis out of the ecliptic, provides a powerful platform for studies of the angular distributions of SEP electrons and ions.** This has been used in studies [Tan *et al.*, 2008, 2009, 2012] to examine the reflection of SEPs at magnetic boundaries produced by earlier CMEs that have now moved out beyond 1 AU. In some events, both ions and electrons are observed as initial beams that flow out along the magnetic field; return beams then appear with a loss-cone distribution somewhat later. The time delay between outward and inward flows can be correlated with the time of passage of a magnetic barrier observed earlier. Magnetic structures can eventually trap a large spatially-uniform population of SEPs with a temporally invariant spectrum in a “reservoir” where the intensities slowly decline adiabatically as the volume of the magnetic bottle expands [Reames, 2013]. Reservoirs have a practical effect on the duration of hazardous radiation from high-energy SEPs.

Tan *et al.* [2011] studied SEP electron scattering and the absorption of resonant waves by the ambient plasma to show why the propagation of relativistic electrons is usually highly diffusive while non-relativistic electrons travel scatter free, with a transition region at energies between.

### SEP Composition Studies

**The use of elemental composition provides a powerful tool to probe the processes that produce SEPs. *Wind*/EPACT has unsurpassed**

collecting power, thus, it has been used to address ongoing controversies of SEP acceleration mechanisms and the sources of event-to-event variability.

*Desai et al.* [2010] combined data from *Wind* and ACE to examine the composition and energy spectra of suprathermal ions during solar-quiet times in 1995-2008. The variation in elemental ratios over the solar cycle explained compositional differences between SEPs and SW plasma, further confirming the preferred role of suprathermal ions as seed particles for shock acceleration. They also found that the energy spectra of the suprathermals exhibit a range of power-law indices, significantly different from some theoretical predictions of a unique 1.5 index.

*Ko et al.* [2012] used the highly-precise *Wind*/EPACT data to investigate event-to-event variability in gradual SEP composition. They found variability that cannot be explained by acceleration or transport effects and therefore comprises another likely signature of differences in the suprathermal seed populations available to the shock. They further found that the compositional signatures were strongly correlated with the strength of the magnetic field at the solar footpoint of the Sun-L1 field line, with stronger fields corresponding to systematic enhancements in heavy-ion composition. These results suggest biases in the seed suprathermals that were generated by magnetic reconnection at the footpoints, thereby illuminating how reconnection and shock-acceleration work together to produce large SEP events.

*Tylka et al.* [2012] revisited the ongoing controversy over the  $\sim 10$ -fold enhancements in the Fe/O ratio sometimes observed in the first few hours of a large, gradual events. These enhancements have been interpreted by various researchers as evidence for a flare-accelerated component or, alternatively, as a signature of rigidity-dependent interplanetary particle transport. By combining modeling with observations of the same events by *Wind*/EPACT (at L1) and by *Ulysses* (at  $>60^\circ$  heliolatitude and beyond 1.6 AU), they demonstrated that the initial Fe/O enhancement is best understood as a transport effect.

*Wind*/EPACT also provided SEP composition data for studies [*Rouillard et al.*, 2011, 2012] that explored SEP characteristics in the context of STEREO CME imaging, and for a systematic study of composition in Ground-Level Events [*Kahler et al.*, 2012a].

### 2.3.3 Anomalous Cosmic Rays (ACRs)

The EPACT/LEMT instrument on *Wind* continues to be an important monitor of 4-20 MeV/n ACR ions, especially He, N, O, Ne, and Ar. These ions began as interstellar neutral atoms that penetrated into the heliosphere, were ionized near the Sun, picked up and carried out by the solar wind, accelerated in the outer

heliosphere, then modulated as they journeyed back to Earth. This modulation of the ACRs differs from that of the galactic cosmic rays (GCRs). Comparison of the time variations of ACRs and GCRs between *Wind* and the *Voyager* spacecraft, especially during the recent, unusually-deep solar minimum [*McDonald et al.*, 2010], help us identify the controversial location of the ACR acceleration.

***Wind* continues to provide a near-Earth ACR baseline for the *Voyager* spacecraft as they move outward during solar cycle 24.** Meanwhile the ACRs continue to support their newly-discovered role as probes of magnetic cloud topology [see Section 2.3.2A *Reames et al.*, 2009].

### 2.3.4 Summary and Relevance

It is important to note that a great deal of the studies presented in Section 2 have resulted from observations relying upon *Wind* alone. It is because of *Wind*'s comprehensive array of instruments and their high time, angular, and energy resolution measurements that *Wind* is able to perform such pioneering studies without significant help from other spacecraft. In particular, the EPACT/LEMT energetic particle measurements continue to provide a unique view of SEP acceleration and transport. In addition, *Wind* is instrumental to numerous other heliospheric missions (see Section 4). **These capabilities make *Wind* one of the most important and highly used near-Earth spacecraft.**

## 3 Prioritized Science Goals

### *Wind* Prioritized Science Goals

1. Long-term variation covering 2 Solar Cycles
  - (a) Solar wind abundance variations
  - (b) SEP variations
2. Acceleration and heating of the solar wind and kinetic physics
3. The inner heliospheric propagation and evolution of ICMEs
  - (a) Local and global distortions of ICME geometry
  - (b) Why do some CMEs evolve into irregular ejecta?
4. Dust science

The *Wind* mission is operating on a minimal budget that does not allow for the dedicated support of any in-depth focus scientific research. The funding is applied to the operation of the spacecraft and the collection and validation of high quality solar wind measurements. While, as part of the instrument data validation process, quite a number of significant scientific discoveries have been made even in recent years as outlined in the previous sections, most detailed scientific research using *Wind* data is primarily supported under ROSES GI and SR&T. In the following sections, we outline a

number of prioritized and focused science research topics that the *Wind* instrument teams are planning to undertake using unique *Wind* observations but mostly relying on these external financial sources.

### 3.1 Two Complete Solar Cycles

In November, 2016, within the time period covered by this proposal, *Wind* will complete 22 years, or one complete solar magnetic cycle, of continuous observations of the solar wind. Long-term solar cycle studies always critically depend on continuous high quality observations preferable from the same instruments to avoid instrument intercalibration issues. The *Wind* solar wind plasma and magnetic field data has shown a remarkable 0.1% stability due to the quality of the instruments and the intercalibration of SWE, 3DP and WAVES plasma frequency observations. The newly recalibrated MFI magnetic field data has also minimized any long-term drift effects. Thus the *Wind* solar wind observations will be uniquely appropriate for the comparison of solar cycle 22 and 23.

#### 3.1.1 Sources of the Solar Wind

As an example of the type of research that will be undertaken, *Kasper et al.* [2007] analyzed *Wind* data from 1994–2004, showed that the solar wind Helium abundance strongly correlated with the sunspot number for slow solar wind conditions but was nearly constant at  $\sim 4.5\%$  for fast streams (see Figure 18). This implies that the fast and slow streams have fundamentally different sources on the Sun. When updating this study with data till 2010 through the recent, unusually deep solar minimum [*Kasper et al.*, 2012], they found that in the new solar cycle (cycle 23), the fast stream showed similar sunspot correlation of the Helium abundance as the slow stream, bringing the earlier interpretation into question.

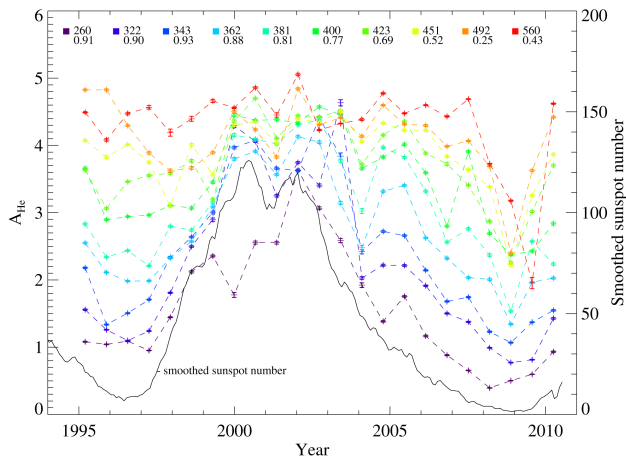


**Figure 18:** Plot of helium relative abundance vs. time for various ranges of solar wind speeds [from Figure 2 in *Kasper et al.*, 2012].

Completing observations through the upcoming solar maximum would allow the direct comparison of so-

lar maximum data from two different cycles. These observations would also allow us to answer questions regarding the dependence of the helium abundance on solar wind speed, which may indicate strong mixing of the solar wind source material.

#### 3.1.2 SEP Variation

Another solar cycle focused science topic will be the variation of the solar energetic particle environment. Though *Wind* does not cover the highest energy ranges for ions (EPACT/LEMT covers 0.04–50 MeV/nuc), it is the only spacecraft measuring the important low to mid energies (below 10 MeV/nuc) with full longitudinal resolution (due to its ecliptic spin plane). *Wind*/3DP also covers energetic electrons to higher energies than any other solar wind spacecraft (up to 500 keV). Future work will compare the occurrence rate, energy spectrum and longitudinal distribution of SEP events between cycle 23 and 24. Of particular import will be to understand the still outstanding question of the sources of solar energetic electrons. Moreover, emphasis will be placed on the study of the spatial and temporal variations at different scales of superhalo electrons in the solar wind, using the *Wind*/3DP and STEREO/STE observations, in order to explore the sources and acceleration of these suprathermal particles.

### 3.2 Heating and Kinetic Physics

*Wind* spacecraft instruments produce the highest time, energy, and angular resolution data in the near-Earth solar wind environment enabling the direct observations wave-particle interactions and plasma instabilities. Recent important discoveries in this regime of kinetic physics, outlined above in Section 2.1, have shown that not only is *Wind* still capable of ground breaking work, the spacecraft has tremendous potential for future discoveries highly relevant for the fundamental heliophysics question of what processes accelerates and heat the solar wind.

The *Wind*/MFI team recently recalibrated the entire magnetic field data set, including spin phase corrections during perigee passes when the spacecraft was in the Earth’s shadow. The recalibration effort resulted in the public release of the highest sample rate data ( $\sim 10$  sps and up to  $\sim 22$  sps when within  $\sim 100 R_E$  of Earth). This nearly untapped new data set will allow for examinations of turbulence theories for nearly two solar cycles to frequencies/scales in the dissipation range where it is believed that waves cascading to ever shorter wavelengths finally are converted into particle heating. This data will also allow for a more detailed examination of solar wind discontinuities where magnetic reconnection tends to operate converting magnetic energy into particle streaming and heating as suggested by a number simulations and some early observations [e.g., *Daughton et al.*, 2011; *Drake et al.*, 2003; *Gosling*, 2007; *Osman et al.*, 2012]. The increased solar activity during the

next couple of years will provide an excellent opportunity to test these theories.

The *Wind*/SWE Faraday Cup (FC) team has recently released enhanced particle velocity moments utilizing the recalibrated  $\sim 3$  second cadence MFI magnetic field data and a constrained density derived from the WAVES/TNR instrument detected electron plasma frequency. The re-calculated anisotropic proton and alpha particle key parameters have already resulted in a re-examination of kinetic instability theories for ion temperature anisotropies in the solar wind [e.g., *Kasper et al.*, 2013]. The SWE team plans to enhance the plasma parameter calculations further by matching each individual energy step measurement to the actual magnetic field direction obtained from the new MFI high time resolution data. This will eliminate time aliasing effects on the  $\sim 92$  second SWE proton measurement cadence and produce dramatic differences in temperature anisotropies for both protons and alpha-particle species. This new data set will improve our understanding of the temperature evolution of the solar wind and the kinetic instabilities that balance anisotropies gaining a crucial insight into solar wind heating even before the *Solar Probe Plus* and *Solar Orbiter* missions will sample the innermost heliosphere.

Recently *Pulupa et al.* [2013] has showed, using the newly reprocessed *Wind*/3DP electron data, that solar wind electron drifts and collisions also significantly contribute to the local heating of the solar wind (see details above in Section 2.1.1). In addition, the unique *Wind*/WAVES instrument is capable measuring the local plasma waves, due to its very long antennas, and even capturing time-domain waveforms with the WAVES/TDS subsystem. The WAVES team is currently finalizing their calibrations for the TDS data, which will provide electromagnetic fields at sub-electron-scale wavelengths for the entire mission. The combination of 3DP electron and TDS plasma wave data affords the opportunity to test turbulence theories and wave-particle interaction processes that operate not only in the 1 AU solar wind, but more crucially in the solar corona. However, these processes occur at even higher frequencies in the corona (due to the stronger magnetic fields and higher plasma densities) making them inaccessible even to the advanced *Solar Probe Plus* instrumentation. Thus, *Wind* will continue to be a unique platform to test coronal and solar wind theories.

### 3.3 The Evolution of ICMEs

The years covered by this proposal will include solar maximum and the declining phase of the current solar cycle, a period when CME activity of the sun dramatically increases. Moreover, during this time period the STEREO spacecraft will be on the far side of the Sun, as seen from Earth, and will cross over in March

2015 and be separated again by  $\sim 112^\circ$  by the end of 2017. Other sources of inner-heliospheric in-situ data are: MESSENGER at planet Mercury ( $\sim 0.3$  AU), VEX at Venus ( $\sim 0.7$  AU), and after September 2014 MAVEN at Mars ( $\sim 1.5$  AU) with *Wind* continuing to monitor the near-Earth environment. Thus, this is a truly unique opportunity in the history of space exploration to have full  $360^\circ$  coverage of the near-ecliptic solar wind in the inner heliosphere allowing multi-spacecraft observations of ICMEs with significantly longitudinal separations.

In this set of focused research topics *Wind* will not be the only or even the primary source of measurements (hence is listed as our third priority), but will provide crucial information. There will be occasions when the longitudinal separation between *Wind* and MESSENGER and/or VEX and MAVEN will be less than the typical longitudinal width of ICMEs (i.e.,  $\sim 60^\circ$ ) allowing in-situ sampling of the same ICME at different radial distances (thus at different evolutionary stages). At the same time, the two STEREO spacecraft will provide white light imaging of the same solar wind structures. This unique configuration and the solar maximum increased CME activity will allow the extension of the white light/in-situ data/modeling studies carried out on a few available ICMEs [e.g., *Nieves-Chinchilla et al.*, 2011, 2012; *Vourlidas et al.*, 2011] answering the questions in the following sections.

#### 3.3.1 Heliospheric Distortions

Recent studies [e.g., *Kahler et al.*, 2012b; *Möstl et al.*, 2012; *Nieves-Chinchilla et al.*, 2012] strongly suggest that ICMEs are significantly deformed by their interaction with the ambient solar wind and with each other by the time to reach 1 AU. Recent advances in the analysis and interpretation of the STEREO HI images and using *Wind* and STEREO Type II radio bursts allows us to follow the ICMEs in the inner heliosphere. Adding in-situ observations from MESSENGER, Venus Express, *Wind* and MAVEN along with occasional energetic electron burst data from *Wind*/3DP to measure the total field line lengths will constrain a newly developed set of global ICME models [e.g., *Hidalgo and Nieves-Chinchilla*, 2012]. The goal of these new, physically more realistic models is to accurately forecast whether an ICME will impinge on Earth and if yes with what geomagnetic impact.

#### 3.3.2 Irregular ICMEs

Another outstanding question is why some CMEs with clear magnetic flux rope signatures in the solar corona become irregular ejecta without any magnetic field organization by the time they reach 1 AU. *Wind* solar wind plasma, and particularly the 3DP and SWE counter streaming electron pitch angle distributions will be critical identifying these irregular structures at 1 AU. The same multi-spacecraft technique described

above will be employed to follow these ICMEs from the Sun. It is believed that a combination of slower ICME speeds and lower internal magnetic flux content along with an inner heliospheric magnetic configuration advantages for rapid magnetic reconnection is responsible for the dissipation of these structures. However, the upcoming multi-spacecraft and multi-instrument observations of a large number of ICMEs will be needed to resolve this issue.

### 3.4 Dust Science

A relatively new area of research for the *Wind* instrument team is dust science. Micron-sized dust particles of interplanetary and interstellar origin frequently strike the *Wind* spacecraft at velocities of a few 10's of km/s [Malaspina et al., 2013b]. Particles vaporize and ionize on impact, creating a plasma cloud near the spacecraft. The cloud perturbs electric fields measured by *Wind*, resulting in high amplitude (up to 500 mV/m), short duration (few ms) spikes. These spikes are observed by the high time resolution *Wind*/TDS waveform receiver [Malaspina et al., 2013b]. Spikes of similar origin have been observed on *Voyager*, *Cassini*, *Vega 1*, *Vega 2*, DS1, and recently on STEREO [Zaslavsky et al., 2012].

*Wind*'s unique combination of fine wire booms, TDS receiver, and spinning geometry allow not only the detection of dust impacts, but also the determination of impact direction [Zaslavsky et al., 2012]. The *Wind*-observed dust flux is consistent with both dedicated dust detector observations of approximately micron-radius particles and micron dust count rates determined from STEREO/WAVES observations [Malaspina et al., 2013b; Zaslavsky et al., 2012] validating the accuracy of these new type of *Wind* observations. *Wind*-observed dust directionality is consistent with contributions from both interstellar and interplanetary dust [Malaspina et al., 2013b]. Interplanetary micron dust is expected to have a nearly isotropic distribution. Interplanetary micron dust is known to travel through the solar system  $\sim 26$  km/s from an approximately fixed direction a few degrees of the ecliptic plane. *Wind*-observed interstellar dust flux should then be modulated by annual variation in the relative velocity vectors of *Wind* (traveling around the Sun with the Earth's orbital velocity of  $\sim 30$  km/s) and the interstellar dust stream. When these vectors add, in March, one expects higher dust flux and clear directionality. When these vectors null one another, in September, one expects lower dust flux and the directionality to be washed out. Dust spikes in *Wind*/TDS data for 2007 were studied, and the predictions above are borne out.

The results of this work suggest that further study of dust observations recorded during *Wind*'s nearly 20 year mission will lead to new insights concerning the characteristics and dynamics of the near-Earth

interplanetary and interstellar dust environment on timescales from a few days and nearly two solar cycles. It is apparent that the full analysis and understanding of the dust impact phenomenon has only just begun. It seems certain that continuing work will provide new understanding of the dust component of our solar system.

## 4 *Wind* Support for Current and Future Missions

As part of the Heliophysics System Observatory (HSO), *Wind* has been contributing to numerous science investigations that rely on multi-spacecraft observations. Many of these have been described in the preceding sections. In addition, *Wind* observations are also critical to many other spacecraft, enabling and enhancing their mission success. This section outlines some of these functions *Wind* serves.

### 4.1 ACE, DSCOVR, and STEREO ACE

*Wind* and ACE have been mutually supporting each other in refining the calibrations of their instrumentation. Since *Wind* determines and inter-calibrates its solar wind plasma measurements from three different instruments that operate based on different physical principles (SWE, 3DP and WAVES), it supplies highly accurate and independent estimates of thermal plasma key parameters. In addition, the SWE instrument can operate through the high-energy particle showers associated with flares and CMEs. Thus the *Wind* data is very robust. The ACE SWEPAM team takes full advantage of these *Wind* solar wind plasma observations to improve their calibrations. This cooperation is expected to continue through the upcoming years.

Magnetic field measurement also mutually benefit from inter-calibrations between *Wind* and ACE. On spinning spacecraft, the highest accuracies are achieved for the spacecraft spin plane components. Since the *Wind* and ACE spin axes are perpendicular, the lower quality, spin axis component calibrations can be improved by comparing them to the appropriate spin plane component from the other spacecraft whenever they are sufficiently close to each other.

Finally, while ACE dominates high energy particle observations, the *Wind*/EPACT/LEMT telescope fills in an important gap in the 1-10 MeV/nucleon range between the ULEIS and SIS instruments on ACE. Since *Wind* is an ecliptic north spinner, unlike ACE detectors, the LEMT instrument also collects anisotropy information of the energetic particle distributions and can detect back-streaming populations from outer heliospheric shocks [e.g., Tan et al., 2009]. Moreover, because of its large collecting area, EPACT can also measure the scientifically interesting smaller prompt solar energetic particle events. **In summary, *Wind* pro-**

**vides significant calibration information to ACE, complements its measurements and facilitates collaborative, multi-spacecraft studies.**

#### DSCOVR

The Deep Space Climate Observatory (DSCOVR) will be launched no earlier than November, 2014 well within the time period covered by this proposal. DSCOVR is tasked to provide solar wind solar wind proton and magnetic field measurements from L1 (the same region where *Wind*, ACE and SoHO operate) for NOAA space weather prediction purposes. DSCOVR will accomplish this by two primary instruments: a Faraday Cup solar wind proton detector and a flux-gate magnetometer, both of which are derivatives of the equivalent instruments on *Wind*. Though DSCOVR is not a NASA science mission and the NOAA measurement requirements are not as strict as those for *Wind* and ACE, every effort will be made to process scientifically useful data from DSCOVR. To accomplish this, ***Wind* Faraday Cup and magnetometer data will be extensively used to intercalibrate the DSCOVR instruments** when the two spacecraft will be in close proximity.

Once fully calibrated, DSCOVR will provide even higher time cadence solar wind ion and magnetic field measurements than *Wind* can produce enabling two point studies of solar wind kinetic physics. For example, the size of reconnection exhausts and X-line current sheets can be determined. Also the special scale over which various wave-particle processes operate will be determined.

#### STEREO

Because *Wind* carries the WAVES and the high time resolution 3DP solar wind experiments, it is the only near-Earth spacecraft that can serve as backup for the STEREO in-situ and radio observations. Together with SoHO, *Wind* can recover all of the scientific objectives of the STEREO mission should one of the twin spacecraft become incapacitated.

Currently, the two STEREO spacecraft and *Wind* are nearly equally displaced from each other in the 1 AU ecliptic plane at  $\sim 120^\circ$ . This configuration is ideal for global heliospheric studies and for the testing of global heliospheric models. The two STEREO spacecraft and SDO image the complete solar surface providing inner boundary conditions from global MHD models. Then *Wind*, along with the two STEREO spacecraft measure the 1 AU in-situ solar wind conditions to validate model predictions at widely displaced positions. With the telemetry rate of the STEREO spacecraft significantly dropping (due to their increasing distance from Earth), the unchanged and continuous *Wind* measurements are becoming even more important. **Thus, *Wind* is in essence the third in-situ “eye” of the STEREO mission.**

#### 4.2 MESSENGER, VEX, and MAVEN

*Wind* observations of the inner heliosphere have recently been complemented by MESSENGER and Venus Express (VEX) in-situ measurements [e.g., Möstl *et al.*, 2012]. MESSENGER has settled into a Mercury orbit. Since the sunward size of the Hermian magnetosphere is much smaller than the MESSENGER orbit radius, MESSENGER returns 0.3 AU solar wind magnetic field measurements at regular intervals. This data has already been successfully used, in conjunction with *Wind* and STEREO measurements to track ICMEs in the inner heliosphere [Nieves-Chinchilla *et al.*, 2012]. VEX, in its extended mission currently approved till at least December, 2014, orbits Venus at 0.76 AU and also spends significant amount of time outside of the magnetosphere of Venus. MAVEN, with a planned late 2013 launch date, will orbit Mars at 1.5 AU, again observing the undisturbed solar wind most of the time. Thus, in the 2014-15 time frame, there will be a unique constellation of four spacecraft spanning 0.3 AU to 1.5 AU that will be able to follow the evolution of solar wind transients. *Wind* will be an important element of this unique constellation.

#### 4.3 Solar Probe Plus and Solar Orbiter

Though Solar Probe Plus (SPP) is not planned to launch till 2018 and Solar Orbiter (SolO) till 2017, thus most of their primary mission outside of the current proposal period, *Wind* is already performing significant studies aiding these future flagship missions. As described in Section 2.1 above, recent *Wind* results identified a solar wind heating process that SPP and SolO will have to verify closer to the Sun. Similar work, our PSG #2, will continued to be carried out. In particular, SPP will be searching for physical processes that are responsible for the heating of the solar corona and the solar wind. These processes tend to take place on very small time scales (e.g., wave-particle interactions, instabilities). **Only the high cadence *Wind* measurements can provide appropriate 1 AU baseline for SPP and SolO observations.** SPP will have an 88 day orbit around the Sun, thus radial and magnetic alignment with *Wind* and with SolO in a 0.3-0.76 AU orbit will be frequent and these three-point studies will significantly enhance the science return of SPP and SolO.

#### 4.4 IBEX and Voyagers

Since the IMP 8 magnetometer stopped returning data in 2000, the *Wind* observations have usually supplied the 1 AU baseline for deep space observations such as those by the Voyagers. **The robust and continuous *Wind* solar wind measurements are essential for studies ranging from the predicted position of the termination shock and heliopause, also observed remotely by IBEX, to the evolution of solar wind transients from the inner heliosphere.**

## 4.5 Magnetospheric Missions

### THEMIS and *Cluster*

Two of the THEMIS spacecraft, called ARTEMIS, are now in permanent lunar orbits spending a large fraction of their time in the ambient solar wind. *Wind*, together with the two ARTEMIS spacecraft, will provide unprecedented multi-point plasma measurements at the uniquely high, 3 second cadence that will address the fundamental question of whether the reconnection X-lines for low magnetic shears are generally patchy or extended. Multi-point high-resolution measurements with *Cluster* and ARTEMIS will also be used to investigate the structure of the reconnection exhaust as a function of the distance from the X-line. It is worth noting that THEMIS used *Wind* to calibrate its ESA plasma instruments [McFadden *et al.*, 2008a,b], since its electric field receivers could not sample high enough frequencies to observe the upper hybrid line consistently.

### *Van Allen Probes* and MMS

The two *Van Allen Probes* launched on August 30, 2012 and the four MMS spacecraft are currently set to launch in October of 2014 (period covered by this Senior Review). In its detailed description of the scientific objectives for the mission, the *Van Allen Probes* Science Working Group has identified a need for solar wind observations to determine the occurrence patterns of the various acceleration, transport, and loss processes for relativistic, near-relativistic, and ring current particles within the Earth's inner magnetosphere. ***Wind* observations of the solar wind plasma and magnetic field will prove ideal for the required magnetospheric input measurements for the *Van Allen Probes* and for the MMS mission.**

## 4.6 RHESSI, *Swift*, and *Fermi*

### RHESSI

RHESSI provides imaging and spectroscopy of the hard X-ray/ $\gamma$ -ray continuum and  $\gamma$ -ray lines emitted by energetic electrons and ions, respectively. RHESSI accurately locates these particles at the Sun, and its precise spectral measurements provide information on the spectra of the parent electrons and ions, and on the ion composition. *Wind*, using the 3DP and EPACT experiments, provides unique in-situ measurements of the energetic electrons and ions that reach  $\sim 1$  AU, and, with WAVES, of the radio emissions produced by the energetic electrons while traveling from the Sun to 1 AU. *Kiplinger* [1995] found that flares with hard X-ray spectra that evolved from soft to hard to harder (SHH) are closely associated with SEP events observed in interplanetary space. These results were later confirmed using a combination of all RHESSI flares and *Wind*/3DP. Namely, all RHESSI flares associated with an SEP event show SHH behavior and none of the flares with SHS behavior are associated with an SEP. While the physical association between the progressively hard-

ening X-ray spectrum and the particles is not understood at present, the results strongly suggest a physical connection between the X-ray-producing electrons in the flare on closed flare loops and the escaping energetic protons on open field lines. This correlation is puzzling and will require further investigations, since it is generally believed that an interplanetary shock front, remote from the flare itself, is the main accelerator. *Wind* will continue to support this and similar RHESSI research projects.

### *Swift* and *Fermi*

Cosmic gamma ray bursts (GRBs) are transients of large red-shift, and take place at least 600 times per year from the entire visible universe. GRBs have time durations of seconds or more, with photon energies ranging from the hard X-ray to very high energy  $\gamma$ -ray. Only 1 GRB is ever seen from any 1 source (since each is presumably a stellar birth/death signal).

Soft gamma repeaters (SGRs) are of somewhat less visible intensity, but with orders of magnitude less absolute magnitude, since their sources are in our Milky Way galaxy and its immediate neighbors, including the Magellanic Clouds. SGRs repeat at random, often or rarely, from a few times up to hundreds of times over spans from days to months. There are only half a dozen known SGR sources.

Giant Flares (GFs) are of greater apparent intensity than GRBs and are very rare, averaging once per decade. GFs are emitted from the source objects of the SGRs, one or none from each source, to date.

The KONUS instrument on *Wind* was designed to study GRBs, SGRs, and GFs, with omnidirectional sensitivity to all  $\gamma$ -ray transients. Its scientific data fall roughly into the following categories: KONUS detects on the average the brightest 120 GRBs per year, thus providing comparison data for many of the *Swift* GRBs. In particular, KONUS provides the higher energy determination that is beyond *Swift*'s energy range. Secondly, KONUS is a key vertex in the Interplanetary GRB Network (IPN), composed of *Swift*, *Fermi*, *Mars Odyssey*, MESSENGER, INTEGRAL, AGILE, *Suzaku*, and HETE-2. The IPN finds the source directions of transients by virtue of its timing geometry, independently of oriented telescopes. KONUS is generally the most sensitive of these to SGRs, an advantage that result from its lack of collimation. Due to the rarity of these astrophysical events, an additional four years of ***Wind* KONUS observations will significantly enhance the events collected by *Swift*, *Fermi* and the IPN.**

## 4.7 *Wind* and CCMC

The Coordinated Community Modeling Center (CCMC) is tasked to validate heliophysics models. In particular, Earth magnetospheric models are driven by solar wind input. The accuracy of this input especially

during extreme solar wind conditions is critical for the proper evaluation of the models. Historically, *Wind* measurements have been used as the standard. It is expected that as future models will become more complex, their sensitivity to input uncertainties will only increase. **Thus continued *Wind* measurements are essential for the CCMC model validation program.**

## 5 Technical Status and Budget

### 5.1 Spacecraft Health

The *Wind* spacecraft continues in very good health. The communication system was successfully reconfigured in 2000 to realize an enhancement in telemetry margin. Reliance on a single digital tape recorder since the 1997 failure of the backup unit has never hampered operations, and measures were taken to minimize its use to extend its life. During the past few years, the spacecraft experienced a few instrument latch-ups and single bit flight software errors most likely due to high energy particle single event upsets. These events served to exercise the spacecraft and instrument recovery procedures and showed that within a day or two, all instruments can be brought back to full science operations.

An examination of the spacecraft power systems shows that the batteries can maintain average bias voltages high enough to exceed the current load shed setting for at least 10 years. In May 2012, all three batteries went through a mode change to reduce the maximum charge voltage. Each battery was experiencing excess charging, causing an increase in temperature and reduction in efficiency. The successful mode changes reduced the temperatures to nominal ranges. There are still six more mode levels available and the last mode change occurred in 2009. The solar array output is producing more than enough current for spacecraft operations and will continue to do so well past 2018. Therefore, *Wind* can operate at current capacity into the next decade.

*Wind* continues to have a large fuel reserve. The latest analysis shows that  $\sim 57$  kg fuel remains, which is equivalent of  $\sim 110$  m/s of radial delta-V assuming normal thruster operations. To maintain its current orbit around the L1 point, *Wind* needs to carry out four station keeping maneuvers every year. These maneuvers are very similar and require  $\sim 0.5$  m/s delta-V each. Thus, barring any other issues, *Wind* can maintain its orbit for nearly 60 years.

### 5.2 Instrument Status

Seven of the eight *Wind* instruments, including all of the fields and particles suits, remain largely or fully functional. The only instrument turned off is the TGRS  $\gamma$ -ray instrument that was designed for only a few years of operations. The general status of all instruments is summarized in Table 2.

The specific degradations in instrument capabilities

are the following: The APE and IT detectors of the EPACT instrument, covering the highest energy ranges, do not work. But the LEMT and STEP telescopes of the same instrument continue to operate normally, providing crucial and unique observations of solar energetic particles up to 10 MeV in energy. On the SMS instrument the SWICS solar wind composition sensor had to be turned off in May 2000. The SMS DPU experienced a latch-up reset on 26 June 2009 that placed the MASS acceleration/deceleration power supply into a fixed voltage mode, rather than stepping through a set of voltages. It has been determined that a moderate risk power cycling of the SMS DPU would be required to fix this problem. In order to protect the unique and fully functional STICS sensor, it has been decided to leave the MASS sensor in a fixed voltage mode that allows reasonable but reduced science data collection. In 2010, MASS experienced a small degradation in the acceleration/deceleration power supply which reduced the efficiency of the instrument, though this does not seriously affect science data analysis.

Finally, the VEIS thermal electron detectors on the SWE instrument experienced high voltage problems in November, 2001. This problem was resolved by reprogramming the SWE Strahl sensor to recover most of the original functions. Moreover, the 3DP instrument also covers the impacted electron measurements making these observations still redundant and hence robust. All of the other instruments continue to function fully.

### 5.3 Science Team

The *Wind* instrument/science team is very small but an extremely dedicated group of scientists. Due to the longevity of the mission, a number of the original instrument PIs have retired (and sadly Bob Lin has unexpectedly passed away) and passed their baton to the next generation. Keith Ogilvie passed the leadership of the SWE instrument suite to Adolfo Vias. Moreover, with the retirement of Al Lazarus at MIT, the SWE Faraday Cup operations are being moved to the Harvard Smithsonian Astrophysical Observatory (SAO) under the guidance of Justin Kasper. With the passing of Bob Lin, Stuart Bale has taken over the PI-ship of 3DP at Berkeley. Adam Szabo has replaced Ron Lepping a number of years ago as the magnetometer PI. Sue Lepri at the University of Michigan is the current PI for SMS, taking over from George Gloeckler. With the retirement of Mike Kaiser, Robert MacDowall is leading the WAVES team. The leadership of EPACT is unchanged though Allan Tylka has very recently officially joined this instrument team. Also, Lynn Wilson has started to serve as the *Wind* Deputy Project Scientist bringing a new level of energy to the project team. The new PIs bring a large number of years of experience with their associated instruments and a high level of enthusiasm to for new discoveries using this venerable spacecraft as

**Table 2:** The status of the *Wind* instruments

Instrument	Principal Investigator	Institution	Status
<b>SWE</b>	A.F- Viñas	Electrons: GSFC, UNH Ions: MIT, SAO	Strahl detector reconfigured Faraday Cup fully operational
<b>3DP</b>	S.D. Bale	UC Berkeley	Fully operational
<b>MFI</b>	A. Szabo	GSFC	Fully operational
<b>SMS</b>	S. Lepri	U. Michigan	SWICS turned off MASS reduced coverage STICS fully operational
<b>EPACT</b>	T. Von Rosenvinge	GSFC	APE and IT turned off LEMT and STEP operational
<b>WAVES</b>	R. MacDowall	GSFC	Fully operational
<b>KONUS</b>	E. Mazets	Ioffe Institute, Russia	Fully operational
<b>TGRS</b>	B. Teegarden	GSFC	Turned off (out of coolant)

the long list of WIND scientific publications testify.

### Students

*Wind* remains a very popular source of solar wind measurements and a rich source of material for PhD work. Ten students received PhDs since the last Senior Review using primarily *Wind* observations: Mike Stevens (MIT, 2009), Linghua Wang (Berkeley, 2009), Lynn Wilson (U. Minnesota, 2010), Mark Pulupa (Berkeley, 2010), E.K.J. Kilpua (Berkeley, 2010), Heli Hietala (U. Helsinki, 2011), Kamen Kozarev (SAO, 2011), Ben Maruca (SAO, 2012), Sonja Vidojevic (U. Paris, 2012), and Yngvild Andalsvik (UNH, 2012). Moreover, Brendan Harris received a Masters degree at UNH in 2010 also using *Wind* data. Currently, six more students are working on their dissertations using *Wind* observations. The university team members also rely on a large number of undergraduate interns to increase their scientific productivity.

### 5.4 Ground Operations

*Wind* ground operations takes place at Goddard and is fully transitioned from the legacy *Polar-Wind-Geotail* system to Multi-Mission Operations Center (MMOC) that consolidates *Wind* operations with that of ACE. This transition became necessary with the decommissioning of Polar on April 30, 2008 and it includes the upgrade of outdated and costly to maintain hardware and software. *Wind* operations were moved to the MMOC on March 11, 2010 and the MMOC Operational Readiness Review was held on March 30, 2010.

For cost saving measures, the flight operations team reduced staffing by 1 FTE in November 2008 and modified shift schedules to reduce operational coverage from twelve to eight hours (reducing the need for overtime and shift differential). With the successful transition of *Wind* flight operations into the MMOC, the staffing levels have been reduced to operate the ACE and *Wind* missions with a combined team that also includes non-traditional flight operations skills (HW/SW maintenance, Flight Dynamics attitude analysis). Re-engineering/upgrading existing systems promoted effi-

ciency with respect to implementing IT Security and HW/ SW maintenance as well as system administration. Automation is being implemented with a unified approach to further increase efficiency. The teams will continue to cross train at multiple positions so that prime and backup roles are covered. In spite of the disruptions due to the transitioning of operation to the MMOC, data recovery for *Wind* for the last two years averaged  $\gtrsim 97.2\%$ . Most of the unrecoverable data loss occurred when *Wind* Deep Space Network supports were released for other spacecraft launches and emergencies with some data loss resulting also from network problems.

The current operation of *Wind* requires one  $\sim 2$  hour DSN support per day. This allows the up-linking of the daily Stored Command Table load and the playback of the Digital Tape Recorder. *Wind* also maintains real-time solar wind monitoring during these 2 hour contacts. In 2001, an attempt was made to reduce the number of DSN contacts, and hence the cost of operations, by scheduling DSN time only once every three days, albeit for longer durations. Reducing the number of contacts saves the lengthy setup and reset times. After extensive testing it was concluded that this scenario did not provide significant savings and introduced critical risks to the mission. *Wind* can store only three days worth of commands, thus this is the longest *Wind* can go without ground contact or the spacecraft performs an emergency load shed. Hence the current flexibility to negotiate contact time with DSN would be eliminated. Also, all of these infrequent contacts would be fully attended regardless of the time of day. Currently about half of the contacts are completely automated allowing the operation staff to keep day schedules. Thus, the current daily contact scenario is considered optimal.

The distribution and archiving of all level zero files and the production of the quick-look key parameter (KP) files also takes place at Goddard, but in the Science Directorate under the control of the project scientist. The two server (plus backup) system was re-

engineered in 2002 and is not expected to require any significant upgrades. Therefore, the servers are expected to remain operational for another 10 years.

## 5.5 In-Guide Budget

The in-guide budget described in this section will fund the mission operations necessary to continue the safe operation of the *Wind* spacecraft along with basic data reduction and validation processes performed at the various instrument institutions. As in the previous years, the scientific research outlined in the previous sections are expected to be funded through the Guest Investigator program with each element individually proposed and peer reviewed.

### 5.5.1 Mission Operations

The inputs in the budget spreadsheet Table II are the direct costs to the *Wind* project. Line 2b is Mission Services calculated by costing the flight operations team at a contractor WYE level of 7.2 for FY14 through FY18. Line 2b includes support from flight dynamics for orbit determination and station keeping maneuvers and the DSN scheduling work. The sustaining engineering cost for FY14-18 is for system administration of the MMOC. Line 2c represents the civil servant salary for a Mission Director, which is charged at 0.2 FTE.

Table IV provides the “In Kind” costs. These are services provide to *Wind* that are funded by other sources. These costs are allocated to *Wind*, but are not supported with Project funds. Line 2a includes the use of the Deep Space Network apertures as well as the cost of voice and data connections at GSFC. Line 2b includes building engineers in the Mission Operations Building at GSFC and Mission Operations and Mission Services (MOMS) contract management costs.

Maintaining the *Wind* portion of the reengineered PWG system will require the support of a software engineer at the 0.2 FTE level. The PWG system is responsible for the archival of the level zero data and its distribution to the instrument sites and for the generation of the quick-look key parameter (KP) data files. Since cost is directly funded from the *Wind* project funds, it is included in Table II line 3, Science Operations Functions. The PWG system hardware requires roughly \$58K/year for FY14–FY18. This cost includes software license fees and are listed in Table III under LZ Production. The overall Goddard project management costs, not including the PWG system, include 0.5 FTE for the deputy project scientist and 0.2 FTE for a contract resource analyst, also carried in Table II on line 3. Note that ~34% of the in-guide funding is needed for mission operations and only ~9% for project management (not including E/PO). Thus, more than half of the *Wind* budget still goes to the instrument teams for data processing and validation.

### 5.5.2 Data Production and Accessibility

The *Wind* science data products are publicly served directly from the instrument team sites (most are directly available from CDAWeb), with a single project web page containing links to and descriptions of the large number of *Wind* data products (<http://wind.nasa.gov>). *Wind* is also an active participant in the development of the Virtual Heliophysics Observatory (VHO) that will make data queries even more user friendly and powerful. Details of the data production are given below.

The other half of the requested in-guide funding is allocated to the generation, calibration and validation of the various *Wind* instrument data products. After receiving the level zero instrument data along with housekeeping and ephemeris information, the instrument teams are responsible for the generation of science quality data that is fully calibrated and validated typically through the performance of well established scientific analysis. In addition, they have to provide full, data granule level description and intermediate-term archiving (i.e., guaranteed backups till final submission to SPDF/CDAWeb). In addition, the occasional *Wind* maneuvers (~4/year for station keeping) necessitate instrument level commanding that the instrument teams are required to support. Thus, besides data production expertise, the teams have to maintain a low level engineering capability that can support routine and emergency operations. Finally, since *Wind* does not have a project level science center, the instrument teams are responsible for the public dissemination of their data through the maintaining of Web pages.

Due to the limited funding available, the instrument teams optimized their operation to stay within ~1 FTE for all aspects of operation. All fully functional instruments (MFI, SWE/Electron, SWE/Faraday Cup, WAVES, 3DP, and EPACT) are allocated almost exactly the same amount of support, regardless whether they are full cost accounted Goddard civil service or university operations. It should be noted that SWE is composed of two independent instruments: the Goddard electron instrument and the MIT Faraday Cup. They each have the same allocation, but are reported together.

The partially functioning instrument (SMS) allocated about half as much as data production requirements are significantly diminished. However, it still continues to produce valuable data, therefore continued support at this reduced level is still requested. The astrophysical KONUS instrument received, in the past, a minimal amount of funding (~\$20K/year) mostly to support project level documentation. This instrument receives some minor amount of funding in Russia for data production and even less support from the *Swift* mission for a part time Goddard contractor. Thus, no

new funding is requested for them in this proposal.

The final budget elements is education and public outreach that is combined for all instruments and is at the  $\sim 1\%$  level of the project total. As it is described in the E/PO section, this funding is proposed to be combined with that of the ACE project for a more substantial effort.

## References

- Belcher, J., and L. Davis Jr. (1971), Large-amplitude Alfvén waves in the interplanetary medium, 2, *J. Geophys. Res.*, *76*, 3534, doi:10.1029/JA076i016p03534.
- Boldyrev, S., and J. Perez (2009), Spectrum of Weak Magnetohydrodynamic Turbulence, *Phys. Rev. Lett.*, *103*, 225,001, doi:10.1103/PhysRevLett.103.225001.
- Boldyrev, S., et al. (2011), Spectral Scaling Laws in Magnetohydrodynamic Turbulence Simulations and in the Solar Wind, *Astrophys. J. Lett.*, *741*, L19, doi:10.1088/2041-8205/741/1/L19.
- Bougeret, J.-L., et al. (1995), Waves: The Radio and Plasma Wave Investigation on the Wind Spacecraft, *Space Sci. Rev.*, *71*, 231–263, doi:10.1007/BF00751331.
- Cairns, I., and B. McMillan (2005), Electron acceleration by lower hybrid waves in magnetic reconnection regions, *Phys. Plasmas*, *12*, 102,110, doi:10.1063/1.2080567.
- Cattell, C., et al. (2008), Discovery of very large amplitude whistler-mode waves in Earth’s radiation belts, *Geophys. Res. Lett.*, *35*, 1105, doi:10.1029/2007GL032009.
- Chen, C., et al. (2013), Residual Energy Spectrum of Solar Wind Turbulence, *Astrophys. J.*, submitted.
- Daughton, W., et al. (2011), Role of electron physics in the development of turbulent magnetic reconnection in collisionless plasmas, *Nature Phys.*, *7*, 539–542, doi:10.1038/nphys1965.
- Desai, M. L., et al. (2010), Origin of Quiet-Time Suprathermal Tails Near 1 AU, *Solar Wind 12*, *1216*, 635–638, doi:10.1063/1.3395946.
- Drake, J., et al. (2003), Formation of Electron Holes and Particle Energization During Magnetic Reconnection, *Science*, *299*, 873–877, doi:10.1126/science.1080333.
- Ebert, R., et al. (2012a), Corotating Interaction Region Associated Suprathermal Helium Ion Enhancements at 1 AU: Evidence for Local Acceleration at the Compression Region Trailing Edge, *Astrophys. J.*, *749*, 73, doi:10.1088/0004-637X/749/1/73.
- Ebert, R., et al. (2012b), Helium Ion Anisotropies in Corotating Interaction Regions at 1 AU, *Astrophys. J. Lett.*, *754*, L30, doi:10.1088/2041-8205/754/2/L30.
- Farrell, W. M., et al. (1995), A method of calibrating magnetometers on a spinning spacecraft, *IEEE Trans. Mag.*, *31*, 966–972, doi:10.1109/20.364770.
- Farrugia, C., et al. (2012), A planar, pressure-balanced, reconnecting structure embedded in a small solar wind transient, *Solar Wind 13*, in press.
- Fisk, L., and M. Lee (1980), Shock acceleration of energetic particles in corotating interaction regions in the solar wind, *Astrophys. J.*, *237*, 620–626, doi:10.1086/157907.
- Ghielmetti, A. G., et al. (1983), Calibration system for satellite and rocket-borne ion mass spectrometers in the energy range from 5 eV/charge to 100 keV/charge, *Rev. Sci. Instr.*, *54*, 425–436, doi:10.1063/1.1137411.
- Gloeckler, G., et al. (1995), The Solar Wind and Suprathermal Ion Composition Investigation on the Wind Spacecraft, *Space Sci. Rev.*, *71*, 79–124, doi:10.1007/BF00751327.
- Gopalswamy, N., et al. (2012), Radio-loud CMEs from the disk center lacking shocks at 1 AU, *J. Geophys. Res.*, *117*, A08106, doi:10.1029/2012JA017610.
- Gosling, J. (2007), Observations of Magnetic Reconnection in the Turbulent High-Speed Solar Wind, *Astrophys. J. Lett.*, *671*, L73–L76, doi:10.1086/524842.
- Gruesbeck, J., et al. (2012), Time Variations of the Suprathermal Distribution as observed by WIND/STICS, *SHINE*, june 25-29, 2012, Hawaii.
- Harrison, R., et al. (2012), An Analysis of the Origin and Propagation of the Multiple Coronal Mass Ejections of 2010 August 1, *Astrophys. J.*, *750*, 45, doi:10.1088/0004-637X/750/1/45.
- Hellinger, P., et al. (2006), Solar wind proton temperature anisotropy: Linear theory and WIND/SWE observations, *Geophys. Res. Lett.*, *33*, 9101, doi:10.1029/2006GL025925.
- Hidalgo, M. A., and T. Nieves-Chinchilla (2012), A Global Magnetic Topology Model for Magnetic Clouds. I., *Astrophys. J.*, *748*, 109, doi:10.1088/0004-637X/748/2/109.
- Hietala, H., et al. (2011), In situ observations of particle acceleration in shock-shock interaction, *J. Geophys. Res.*, *116*, 10,105, doi:10.1029/2011JA016669.
- Hietala, H., et al. (2012), Particle Acceleration in Shock-Shock Interaction: Model to Data Comparison, *Astrophys. J. Lett.*, *751*, L14, doi:10.1088/2041-8205/751/1/L14.
- Jian, L., et al. (2012), Solar wind observations at STEREO: 2007–2011, *Solar Wind 13*, in press.
- Kahler, S. W., et al. (2011), Magnetic Field-line Lengths in Interplanetary Coronal Mass Ejections Inferred from Energetic Electron Events, *Astrophys. J.*, *736*, 106, doi:10.1088/0004-637X/736/2/106.
- Kahler, S. W., et al. (2012a), A Comparison of Ground Level Event e/p and Fe/O Ratios with Associated Solar Flare and CME Characteristics, *Space Sci. Rev.*, *171*, 121–139, doi:10.1007/s11214-011-9768-x.

- Kahler, S. W., et al. (2012b), Deflections of Fast Coronal Mass Ejections and the Properties of Associated Solar Energetic Particle Events, *Astrophys. J.*, *754*, 100, doi:10.1088/0004-637X/754/2/100.
- Kasper, J., et al. (2006), Physics-based tests to identify the accuracy of solar wind ion measurements: A case study with the Wind Faraday Cups, *J. Geophys. Res.*, *111*, 3105, doi:10.1029/2005JA011442.
- Kasper, J., et al. (2007), Solar Wind Helium Abundance as a Function of Speed and Heliographic Latitude: Variation through a Solar Cycle, *Astrophys. J.*, *660*, 901–910, doi:10.1086/510842.
- Kasper, J., et al. (2013), Sensitive test for ion-cyclotron resonant heating in the solar wind, *Phys. Rev. Lett.*, *110*, accepted Jan. 11, 2013.
- Kasper, J. C., et al. (2012), Evolution of the Relationships between Helium Abundance, Minor Ion Charge State, and Solar Wind Speed over the Solar Cycle, *Astrophys. J.*, *745*, 162, doi:10.1088/0004-637X/745/2/162.
- Kellogg, P., et al. (2010), Electron trapping and charge transport by large amplitude whistlers, *Geophys. Res. Lett.*, *37*, 20,106, doi:10.1029/2010GL044845.
- Kellogg, P., et al. (2011), Large amplitude whistlers in the magnetosphere observed with Wind-Waves, *J. Geophys. Res.*, *116*, A09,224, doi:10.1029/2010JA015919.
- Kersten, K., et al. (2011), Observation of relativistic electron microbursts in conjunction with intense radiation belt whistler-mode waves, *Geophys. Res. Lett.*, *38*, 8107, doi:10.1029/2011GL046810.
- Kiplinger, A. (1995), Comparative Studies of Hard X-Ray Spectral Evolution in Solar Flares with High-Energy Proton Events Observed at Earth, *Astrophys. J.*, *453*, 973, doi:10.1086/176457.
- Ko, Y.-K., et al. (2012), On the relationship between heavy-ion composition variability in gradual SEP events and the associated IMF source regions, in *In: Space Weather: The Space Radiation Environment, AIP Conf. Ser.*, vol. 1500, edited by Q. Hu et al., pp. 26–31, doi:10.1063/1.4768740.
- Koval, A., and A. Szabo (2010), Multispacecraft observations of interplanetary shock shapes on the scales of the Earth’s magnetosphere, *J. Geophys. Res.*, *115*, 12,105, doi:10.1029/2010JA015373.
- Lepping, R. P., et al. (1995), The Wind Magnetic Field Investigation, *Space Sci. Rev.*, *71*, 207–229, doi:10.1007/BF00751330.
- Lin, R. P., et al. (1995), A Three-Dimensional Plasma and Energetic Particle Investigation for the Wind Spacecraft, *Space Sci. Rev.*, *71*, 125–153, doi:10.1007/BF00751328.
- Malaspina, D., et al. (2013a), Electrostatic Solitary Waves in the Solar Wind: Evidence for Instability at Solar Wind Current Sheets, *J. Geophys. Res.*, doi: 10.1029/2012JA018298, in press.
- Malaspina, D., et al. (2013b), Interplanetary and Interstellar Dust as Observed by Wind/WAVES Electric Field Antennas, *Geophys. Res. Lett.*, in preparation.
- Maruca, B., et al. (2011), What Are the Relative Roles of Heating and Cooling in Generating Solar Wind Temperature Anisotropies?, *Phys. Rev. Lett.*, *107*, 201,101, doi:10.1103/PhysRevLett.107.201101.
- Maruca, B., et al. (2012), Instability-driven Limits on Helium Temperature Anisotropy in the Solar Wind: Observations and Linear Vlasov Analysis, *Astrophys. J.*, *748*, 137, doi:10.1088/0004-637X/748/2/137.
- McDonald, F. B., et al. (2010), Unusual time histories of galactic and anomalous cosmic rays at 1 AU over the deep solar minimum of cycle 23/24, *Geophys. Res. Lett.*, *37*, L18101, doi:10.1029/2010GL044218.
- McFadden, J., et al. (2008a), The THEMIS ESA Plasma Instrument and In-flight Calibration, *Space Sci. Rev.*, *141*, 277–302, doi:10.1007/s11214-008-9440-2.
- McFadden, J., et al. (2008b), THEMIS ESA First Science Results and Performance Issues, *Space Sci. Rev.*, *141*, 477–508, doi:10.1007/s11214-008-9433-1.
- Möstl, C., et al. (2012), Multi-point Shock and Flux Rope Analysis of Multiple Interplanetary Coronal Mass Ejections around 2010 August 1 in the Inner Heliosphere, *Astrophys. J.*, *758*, 10, doi:10.1088/0004-637X/758/1/10.
- Nieves-Chinchilla, T., et al. (2011), Analysis and study of the in situ observation of the June 1st 2008 CME by STEREO, *J. Atmos. Solar-Terr. Phys.*, *73*, 1348–1360, doi:10.1016/j.jastp.2010.09.026.
- Nieves-Chinchilla, T., et al. (2012), Remote and in situ observations of an unusual Earth-directed coronal mass ejection from multiple viewpoints, *J. Geophys. Res.*, *117*, 6106, doi:10.1029/2011JA017243.
- Ogilvie, K. W., et al. (1995), SWE, A Comprehensive Plasma Instrument for the Wind Spacecraft, *Space Sci. Rev.*, *71*, 55–77, doi:10.1007/BF00751326.
- Osman, K., et al. (2012), Kinetic Signatures and Intermittent Turbulence in the Solar Wind Plasma, *Phys. Rev. Lett.*, *108*, 261,103, doi:10.1103/PhysRevLett.108.261103.
- Pulupa, M., et al. (2010), Langmuir waves upstream of interplanetary shocks: Dependence on shock and plasma parameters, *J. Geophys. Res.*, *115*, 4106, doi: 10.1029/2009JA014680.
- Pulupa, M., et al. (2011), An asymmetry of the electron foreshock due to the strahl, *Geophys. Res. Lett.*, *38*, 14,105, doi:10.1029/2011GL048029.
- Pulupa, M., et al. (2013), Monopole-dipole spacecraft potential: observations and effects on electron moments, *J. Geophys. Res.*, in preparation.
- Reames, D. V. (2009a), Solar Release Times of Energetic Particles in Ground-Level Events, *Astrophys.*

- J.*, 693, 812–821, doi:10.1088/0004-637X/693/1/812.
- Reames, D. V. (2009b), Solar Energetic-Particle Release Times in Historic Ground-Level Events, *Astrophys. J.*, 706, 844–850, doi:10.1088/0004-637X/706/1/844.
- Reames, D. V. (2010), Remote Sensing of Magnetic-Cloud Topology, *Solar Phys.*, 265, 187–195, doi:10.1007/s11207-010-9527-2.
- Reames, D. V. (2012), Particle Energy Spectra at Traveling Interplanetary Shock Waves, *Astrophys. J.*, 757, 93, doi:10.1088/0004-637X/757/1/93.
- Reames, D. V. (2013), The Two Sources of Solar Energetic Particles, *Space Sci. Rev.*, pp. 1–40, doi:10.1007/s11214-013-9958-9.
- Reames, D. V., and C. K. Ng (2010), Streaming-limited Intensities of Solar Energetic Particles on the Intensity Plateau, *Astrophys. J.*, 723, 1286–1293, doi:10.1088/0004-637X/723/2/1286.
- Reames, D. V., et al. (2009), Anomalous Cosmic Rays as Probes of Magnetic Clouds, *Astrophys. J. Lett.*, 700, L196–L199, doi:10.1088/0004-637X/700/2/L196.
- Richardson, I. (2004), Energetic Particles and Corotating Interaction Regions in the Solar Wind, *Space Sci. Rev.*, 111, 267–376, doi:10.1023/B:SPAC.0000032689.52830.3e.
- Richardson, I., and H. Cane (2010), Near-Earth Interplanetary Coronal Mass Ejections During Solar Cycle 23 (1996 - 2009): Catalog and Summary of Properties, *Solar Phys.*, 264, 189–237, doi:10.1007/s11207-010-9568-6.
- Richardson, I., and H. Cane (2011a), Galactic Cosmic Ray Intensity Response to Interplanetary Coronal Mass Ejections/Magnetic Clouds in 1995 - 2009, *Solar Phys.*, 270, 609–627, doi:10.1007/s11207-011-9774-x.
- Richardson, I., and H. Cane (2011b), Geoeffectiveness (Dst and Kp) of interplanetary coronal mass ejections during 1995-2009 and implications for storm forecasting, *Space Weather*, 9, 7005, doi:10.1029/2011SW000670.
- Riley, P., and N. Crooker (2004), Kinematic Treatment of Coronal Mass Ejection Evolution in the Solar Wind, *Astrophys. J.*, 600, 1035–1042, doi:10.1086/379974.
- Riley, P., et al. (2004), Fitting flux ropes to a global MHD solution: a comparison of techniques, *J. Atmos. Solar-Terr. Phys.*, 66, 1321–1331, doi:10.1016/j.jastp.2004.03.019.
- Rouillard, A. P., et al. (2011), Interpreting the Properties of Solar Energetic Particle Events by Using Combined Imaging and Modeling of Interplanetary Shocks, *Astrophys. J.*, 735, 7, doi:10.1088/0004-637X/735/1/7.
- Rouillard, A. P., et al. (2012), The Longitudinal Properties of a Solar Energetic Particle Event Investigated Using Modern Solar Imaging, *Astrophys. J.*, 752, 44, doi:10.1088/0004-637X/752/1/44.
- Santolík, O., et al. (2010), Survey of Poynting flux of whistler mode chorus in the outer zone, *J. Geophys. Res.*, 115, 0, doi:10.1029/2009JA014925.
- Savani, N., et al. (2011), Evolution of Coronal Mass Ejection Morphology with Increasing Heliocentric Distance. I. Geometrical Analysis, *Astrophys. J.*, 731, 109, doi:10.1088/0004-637X/731/2/109.
- Tan, L. C., et al. (2008), Ion Anisotropy and High-Energy Variability of Large Solar Particle Events: A Comparative Study, *Astrophys. J.*, 678, 1471–1479, doi:10.1086/533490.
- Tan, L. C., et al. (2009), Observational Evidence on the Presence of an Outer Reflecting Boundary in Solar Energetic Particle Events, *Astrophys. J.*, 701, 1753–1764, doi:10.1088/0004-637X/701/2/1753.
- Tan, L. C., et al. (2011), What Causes Scatter-free Transport of Non-relativistic Solar Electrons?, *Astrophys. J.*, 728, 133, doi:10.1088/0004-637X/728/2/133.
- Tan, L. C., et al. (2012), Use of Incident and Reflected Solar Particle Beams to Trace the Topology of Magnetic Clouds, *Astrophys. J.*, 750, 146, doi:10.1088/0004-637X/750/2/146.
- Tylka, A., et al. (2012), Initial Fe/O Enhancements in Large, Gradual, Solar Energetic Particle Events: Observations from Wind and Ulysses, *Solar Phys.*, p. 172, doi:10.1007/s11207-012-0064-z.
- Vasanth, V., and S. Umapathy (2013), A Statistical Study on CMEs Associated with DH-Type-II Radio Bursts Based on Their Source Location (Limb and Disk Events), *Solar Phys.*, 282, 239–247, doi:10.1007/s11207-012-0126-2.
- von Rosenvinge, T. T., et al. (1995), The Energetic Particles: Acceleration, Composition, and Transport (EPACT) investigation on the WIND spacecraft, *Space Sci. Rev.*, 71, 155–206, doi:10.1007/BF00751329.
- Vourlidas, A., et al. (2011), The First Observation of a Rapidly Rotating Coronal Mass Ejection in the Middle Corona, *Astrophys. J. Lett.*, 733, L23, doi:10.1088/2041-8205/733/2/L23.
- Wang, L., et al. (2012), Quiet-time Interplanetary ~20 keV Superhalo Electrons at Solar Minimum, *Astrophys. J. Lett.*, 753, L23, doi:10.1088/2041-8205/753/1/L23.
- Weygand, J., et al. (2013), Magnetic Correlation Functions in the Slow and Fast Solar Wind in the Eulerian Reference Frame, *J. Geophys. Res.*, submitted.
- Wilson III, L. B., et al. (2010), Large-amplitude electrostatic waves observed at a supercritical interplanetary shock, *J. Geophys. Res.*, 115, 12,104, doi:10.1029/2010JA015332.

- Wilson III, L. B., et al. (2011), The properties of large amplitude whistler mode waves in the magnetosphere: propagation and relationship with geomagnetic activity, *Geophys. Res. Lett.*, *38*, L17,107, doi:10.1029/2011GL048671.
- Wilson III, L. B., et al. (2012), Observations of Electromagnetic Whistler Precursors at Supercritical Interplanetary Shocks, *Geophys. Res. Lett.*, *39*, L08,109, doi:10.1029/2012GL051581.
- Wilson III, L. B., et al. (2013a), Electromagnetic waves and electron anisotropies downstream of supercritical interplanetary shocks, *J. Geophys. Res.*, *118*, 1–11, doi:10.1029/2012JA018167.
- Wilson III, L. B., et al. (2013b), Shocklets, SLAMS, and field-aligned ion beams in the terrestrial foreshock, *J. Geophys. Res.*, doi:10.1029/2012JA018186, in press.
- Wu, C. (1984), A fast Fermi process - Energetic electrons accelerated by a nearly perpendicular bow shock, *J. Geophys. Res.*, *89*, 8857–8862, doi:10.1029/JA089iA10p08857.
- Xie, H., et al. (2012), Understanding shock dynamics in the inner heliosphere with modeling and Type II radio data: The 2010-04-03 event, *J. Geophys. Res.*, *117*, A04105, doi:10.1029/2011JA017304.
- Zaslavsky, A., et al. (2012), Interplanetary dust detection by radio antennas: Mass calibration and fluxes measured by STEREO/WAVES, *J. Geophys. Res.*, *117*, 5102, doi:10.1029/2011JA017480.

## A Mission Archive Plan

Early in its mission, *Wind* and the other GGS spacecraft relied on a very capable and extensive science operations center, the Science Planning and Operations Facility (SPOF). The SPOF was responsible for the collecting, distribution and active archiving of all level zero (LZ) and ancillary data products. The SPOF also ran daily the instrument team provided data processing software to produce quick turnaround, publicly available data, termed Key Parameters (KPs). The SPOF also provided science planning and software maintenance services.

With the passage of time, and with reducing funding levels, the SPOF had to be turned off and most of its functions were passed on to the instrument teams and to a small operation, the *Polar-Wind-Geotail* or PWG system, that continued to perform some LZ and KP functions. This unavoidable decentralization resulted in a degree of unevenness and disparity between the various *Wind* instrument data services. To solve this problem, key *Wind* instrument team members rallied around the new distributed Heliophysics Data Environment (HDE) concept and became funding members of the Virtual Heliospheric Observatory (VHO). The VHO provides a single point of entry for data location without the costly necessity of a dedicated science operations center. As a byproduct, *Wind* instrument data were among the first to be fully documented with the common SPASE dictionary based metadata standard thus providing the user community an even level of descriptions of instruments and data products.

### Mission Operations Center

*Wind* ground operations takes place at Goddard and is fully transitioned from the legacy PWG system to Multi-Mission Operations Center (MMOC) that consolidates *Wind* operations with that of ACE. This transition became necessary with the decommissioning of Polar on April 30, 2008 and it includes the upgrade of outdated and costly to maintain hardware and software. *Wind* operations were moved to the MMOC on March 11, 2010 and the MMOC Operational Readiness Review was held on March 30, 2010.

The primary responsibility of the MMOC is spacecraft commanding, trend and anomaly analysis, DSN scheduling, the maintenance of *Wind* Near-Real-Time (NRT) passes and LZ generation for each instrument and spacecraft housekeeping. In addition, the Goddard flight dynamics facility provides orbit and attitude solutions to the MMOC. The MMOC, in turn, sends all of these data products daily to the PWG system.

### The PWG System

The *Polar-Wind-Geotail* (PWG) system handles the active archiving of LZ and ancillary files and their distribution to the instrument teams and various active archives. The PWG system also performs the rapid KP data production for all instruments. It resides also at Goddard but with the team of the project scientist. The PWG system has been streamlined onto only two computers (a data server and a data processor, with hot spares) and is fully automated to eliminate the need for data technicians. The system is maintained by one civil service IT engineer at a fraction of FTE. This system also serves as the interface to the *Wind* NRT data stream, which is real-time processed data during the daily ~2 hour long spacecraft telemetry contact times. This NRT data is available in numerical and graphical format at: <http://pwg.gsfc.nasa.gov/windnrt/>.

The PWG system distributes the instrument and spacecraft housekeeping LZ files to the instrument teams via FTP. All of these LZ and orbit/attitude files are also publicly accessible at <ftp://pwgdata.gsfc.nasa.gov/pub/>. Only the most recent 60 days are served in uncompressed format, but the whole mission is archived in GZip compression. Even though the deep archival of these data files are handled by SPDF, the PWG system also backs up all LZ data at two physical locations and onto CDAWeb. It should be noted that the whole *Wind* mission to date requires only 300GB of storage for the LZ data, so the backup requirements are not overwhelming.

At the beginning of the mission, all *Wind* instrument teams had to supply software to automatically process some portion of their data into science data products, the KP data. Even though the KP data is clearly not the best quality data the instrument teams produce, because it is always available publicly within 24 hours of observation, it enjoys great popularity. The PWG system maintains this software library, with occasional support (as needed) from the instrument teams and automatically places all the KP data on <http://cdaweb.gsfc.nasa.gov>. A more detailed description of the various KP products is given at the instrument sections below.

The PWG system also keeps the Satellite Situation Center (SSCWeb) up to date with orbit information (<http://sscweb.gsfc.nasa.gov>). Thus, all orbit graphics generated on SSCWeb are always up to date.

### Instrument Data

The bulk of the instrument data dissemination takes place through CDAWeb that also serves as the *Wind* Active Archive. To aid the user community, we also developed a *Wind* project web page (<http://wind.nasa.gov>) that identifies the entry point for each instrument data environment and provides some degree of common documentation. The *Wind* project web page includes an updated list of publications and a link to the *Wind* Wikipedia web page ([http://en.wikipedia.org/wiki/WIND\\_\(spacecraft\)](http://en.wikipedia.org/wiki/WIND_(spacecraft))) that we developed. Most of the *Wind*

data products can also be searched, down to the parameter level, through VHO providing rapid access to a wide range of events in the very long duration *Wind* data set. Next we detail the data product status of each *Wind* instrument.

### SWE Ions

*Documentation:* The SWE Faraday Cup (FC) sub-system was designed to measure solar wind thermal protons and positive ions. The physical sensor is completely described in the Space Science Review article *Ogilvie et al.* [1995]. This article was also reproduced in the Global Geospace Mission book and portions of it are available through the *Wind* project web page (<http://wind.nasa.gov>).

The data production procedures are described by *Ogilvie et al.* [1995], but a much more detailed discussion is provided by J.C. Kasper in his PhD dissertation. The relevant chapters are reproduced on the *Wind* project web page. While error analysis results are included in each FC data file, the systematic uncertainties of the measurements, calibrated against other *Wind* instruments and based on basic physical principles, are discussed in *Kasper et al.* [2006]. This paper is also available on the *Wind* project web page.

*Data Products:* The PWG system, on receipt of the LZ data, immediately processes a KP data product for SWE/FC. This automated procedure uses a convected isotropic Maxwellian to fit to the reduced distribution functions collected by the FC. These 92-second time resolution ASCII data files are available to the public within 24 hours of the observations at the MIT instrument web site ([http://web.mit.edu/space/www/wind/wind\\_data.html](http://web.mit.edu/space/www/wind/wind_data.html)) and at CDAWeb (<http://cdaweb.gsfc.nasa.gov>). One hour averages of this data is also available at the MIT instrument page. While the KP products were originally designed as browse, quick look data, the quality proved to be so high that this data product became a frequently used science level data product of the FC sub-system.

Recently, a new data production algorithm was developed that employs a bi-Maxwellian fit and obtains anisotropic temperatures for protons and a separate fit for Alpha particles. The resulting data product (designated H1 by CDAWeb), also contains the simpler moment computations primarily to allow direct comparison with the ACE SWEPAM proton data. This 92-second time resolution data can be located in CDF format at CDAWeb. The whole mission, since 1994 has been reprocessed with this new algorithm and is available generally till 2-3 months behind real time as it requires the final calibrated MFI magnetic field data that needs several months to be computed.

Two new FC data products are being considered for development. During most of its 92-second cycle through the energy steps, the rotating FC data can be used to generate 3-second time resolution proton measurements. Test runs have demonstrated this algorithm, but since this is intrinsically not a continuous data product and since the 3DP instrument already produces 3-second proton data, the generation of this new FC data product is of low priority and is primarily a backup to the 3DP data. Of much higher priority is the generation of the reduced distribution functions in physical units with all instrument effects folded in. Obviously, this data exists (this is what is fitted for the KP and H1 data) but is internal to the data production software. Due to its complexity on a rotating platform, this information was originally not planned to be publicly distributed. However, recently – encouraged by the development of new metadata standards that can handle complex data sets – the generation of the reduced distribution functions was reinvestigated. This would be the most fundamental and complete presentation of the FC measurements. It is however, a major undertaking, and at the current low funding level of the instruments, it proceeds at a very slow pace. It is our plan that within two years this new data will be fully tested and made publicly available.

All of the FC data products are archived at the SPDF active archive and at NSSDC. The FC data products are summarized in the table below.

SWE Ion Data	Cadence	Coverage	Format	Location
KP Protons (K0)	92 s	1994/11/17–Present	ASCII CDF	MIT <sup>a</sup> , FTPHelper <sup>b</sup> CDAWeb <sup>c</sup>
KP Protons	1 hr	1994/11/17–Present	ASCII	MIT
Bi-Maxwellian (H1)	92 s	1995/01/01–Present <sup>d</sup>	ASCII CDF	MIT CDAWeb

<sup>a</sup> [http://web.mit.edu/space/www/wind/wind\\_data.html](http://web.mit.edu/space/www/wind/wind_data.html);

<sup>b</sup> <http://ftpbrowser.gsfc.nasa.gov>;

<sup>c</sup> <http://cdaweb.gsfc.nasa.gov>;

<sup>d</sup> ~6 month lag

### SWE Electrons

*Documentation:* The SWE electron sub-system consists of two electrostatic analyzers, the vector spectrometer (VEIS) and the Strahl spectrometer. They were designed to measure the solar wind electron distribution function. The sensors are fully described by *Ogilvie et al.* [1995] and the instrument description portion of this paper can also be found at the *Wind* project web page (<http://wind.nasa.gov>).

Due to a high voltage supply failure the last available data from the VEIS detector is May 31, 2001. Since the Strahl detector has very similar capabilities (though it was used in a different manner at the beginning of the mission) it was reprogrammed and the ground software rewritten to recover the electron moment and pitch angle measurements originally supplied by VEIS. The SWE Space Science Review article has been updated with these modifications and is available at the *Wind* project page along with a technical description of the new ground software algorithms. Moreover, the headers of the CDF data files have extensive documentation for each data product.

*Data Products:* There are four SWE electron data products: (1) electron moments containing electron density, velocity, temperature and heat flux parameters; (2) the pitch angle files providing electron fluxes at 30 directional bins relative to the instantaneous magnetic field direction at 13 different energy levels; (3) the averaged pitch angle data product with various aggregate averages formed from the complete pitch angle data; (4) and finally the strahl data with higher angular resolution electron pitch angle observations near the magnetic field direction. Starting on Aug 16, 2002, all of these four data products are generated by the new production software based on the reprogrammed Strahl detector measurements. In addition, the electron “moments” are no longer the result of integral moment calculations but estimated from the fitting of a single kappa distribution function to both the core and halo components. Except for the Strahl data, all electron data products are available through CDAWeb. The strahl data is available from the instrument web page. The current availability of the SWE electron data products is summarized in the table below.

SWE Electron Data	Cadence	Coverage	Format	Location
Moments (H0)	12 s	1994/12/29–2001/05/31	CDF	SWEFTP <sup>a</sup> , CDAWeb <sup>b</sup>
Pitch-angle (H4)	12 s	1994/12/29–2001/05/31	CDF	SWEFTP, CDAWeb
Avg. Pitch-angle (M2)	12 s	1994/12/29–2001/05/31	CDF	SWEFTP, CDAWeb
Strahl	12 s	1994/12/29–2001/05/31	binary	SWEFTP
New Moments (H5)	12-15 s	2002/08/16–Present	CDF	SWEFTP, CDAWeb
New Pitch-angle (H3)	12-15 s	2002/08/16–Present	CDF	SWEFTP, CDAWeb
New Avg. Pitch-angle (M0)	12-15 s	2002/08/16–Present	CDF	SWEFTP, CDAWeb
New Strahl	12-15 s	2002/08/16–Present	CDF	SWEFTP

<sup>a</sup> <ftp://windswe.gsfc.nasa.gov/pub>;

<sup>b</sup> <http://cdaweb.gsfc.nasa.gov>

### 3DP

*Documentation:* The *Wind*/3DP instrument consists of six different sensors. There are two electron (EESA) and two ion (PESA) electrostatic analyzers with different geometrical factors and fields-of-view. This way, they can cover the wide dynamic range from 3 eV to 30 keV that encompasses the bulk of the solar wind and much lower density suprathermal populations. There are also a pair of solid state telescopes (SST) the measure electrons with energies up to 400 keV and protons with energies up to 6 MeV. The instrument is fully described by *Lin et al.* [1995]. The instrument description portion of this paper is reproduced at the *Wind* project web site.

The PESA and EESA detectors are swept over their energy range typically 32 times per the 3-second spacecraft spin rate to produce very high time resolution 3D distributions. This process results in a very large volume of data that cannot all be telemetered to the ground. Thus, extensive use is made of on-board processing capabilities. As a result a large number of 3DP data products were developed, some based on on-board processing and some generated on the ground. Some documentation of these data products exist at the 3DP instrument web page (<http://sprg.ssl.berkeley.edu/wind3dp/>). Extensive 3DP metadata can also be publicly located on VHO.

*Data Products:* As most *Wind* instruments, 3DP team has provided a KP production software to be run automatically at the PWG system. This data product contains electron and ion fluxes at seven energies for each particle and some basic moment computations and can be found at CDAWeb for the whole duration of the mission. Much more popular is the unique 3 second time resolution proton moment (PM) data. Even though it is computed on-board the spacecraft, as a result of the recently updated calibration tables uploaded,

it has proven very reliable. It can be accessed for the complete mission at both the 3DP instrument site and at CDAWeb. In addition, the 24-second time resolution ion omni-directional fluxes and the 98-second electron omni-directional fluxes can also be obtained at both the 3DP and CDAWeb sites along with the electron pitch angle distributions. The proton pitch angle distributions and SST energy spectra are currently available only at the 3DP site. However, work is already ongoing to transfer these data sets also to CDAweb.

The current status of the 3DP data products is listed in the table below. All of them cover the full mission duration from 1994/11/15 to present.

3DP Data Product	Cadence	Coverage	Format	Location
KP	92 s	Entire Mission	CDF	CDAWeb <sup>a</sup>
PM <sup>b</sup>	3 s	Entire Mission	CDF	CDAWeb, Berkeley <sup>c</sup>
ELSP <sup>d</sup>	24-98 s	Entire Mission	CDF	CDAWeb, Berkeley
PLSP <sup>e</sup>	24 s	Entire Mission	CDF	CDAWeb, Berkeley
ELPD <sup>f</sup>	24-98 s	Entire Mission	CDF	CDAWeb, Berkeley
PLPD	24 s	Entire Mission	CDF	Berkeley
SFSP SST <sup>g</sup>	12 s	Entire Mission	CDF	Berkeley
SOSP SST <sup>h</sup>	12 s	Entire Mission	CDF	Berkeley

<sup>a</sup> <http://cdaweb.gsfc.nasa.gov>; <sup>b</sup> on-board proton moments; <sup>c</sup> <http://sprg.ssl.berkeley.edu/wind3dp>; <sup>d</sup> EL = electron, SP = omni directional fluxes; <sup>e</sup> PL = proton; <sup>f</sup> PD = pitch-angle; <sup>g</sup> SF = foil (electrons), SST = solid state telescope; <sup>h</sup> SO = open (protons)

## SMS

*Documentation:* The *Wind* SMS instrument suite is composed of three separate instruments. The SupraThermal Ion Composition Spectrometer (STICS) determines mass, mass per charge, and energy for ions in the energy range from 6-230 keV/e. The high resolution mass spectrometer (MASS) determines elemental and isotopic abundances from ~0.5-12 keV/e. Finally, the Solar *Wind* Ion Composition Spectrometer (SWICS) experienced a failure of the “stop” MCP and hence has reduced capabilities. Initially, it provided mass, charge, and energy for ions in the energy range of ~0.5-30 keV/e. However, since the failure the particles mass and charge cannot be uniquely determined and no data is currently processed from it. These instruments are fully described by *Gloeckler et al.* [1995]. The Instrument calibration is fully described by *Ghielmetti et al.* [1983] and in the PhD thesis of K. Chotoo both available at the *Wind* project page. Additional data release notes are archived at the VHO.

SMS Data Product	Cadence	Coverage	Format	Location
KP SWICS+STICS	4 hr	1994/12/12–2000/05/27	CDF	CDAWeb <sup>a</sup>
STICS <sup>b</sup>	1 day	1995/01/01–2007/12/31	ASCII	<i>Wind</i> Project <sup>c</sup>
SWICS+MASS <sup>d</sup>	1 hr	Select Days	ASCII	UMichigan <sup>e</sup>

<sup>a</sup> <http://cdaweb.gsfc.nasa.gov>; <sup>b</sup> proton and alpha-particle distribution functions; <sup>c</sup> <http://wind.nasa.gov>; <sup>d</sup> energy spectra; <sup>e</sup> <http://pooh.engin.umich.edu/wind/>

*Data Products:* Till the failure of the SWICS instrument (May 27, 2000), combined SWICS and STICS KP files were generated that contain alpha particle information along with some carbon and oxygen abundances and temperatures. This data product is still publicly available from CDAWeb. Since the SWICS failure, a lot of time went into determining how to properly use the other two sensors by themselves. A new software system has been developed which automates many data analysis functions previously done manually. This system first simultaneously assigns events to specific ion species, removing any overlap and using the statistical properties of the measurements to maximum advantage. It then uses these assigned events to construct phase space density distribution functions and corrects these for the effects of instrument efficiency and sampling geometry. Finally, it outputs these distribution functions, error estimates, and count rates for each ion along with many intermediate products that facilitate detailed analysis. The software can perform arbitrary time integrations of the data and can optionally use an inversion method to remove overlap among ions in the instrument measurement space. Development of this system is in the data validation and optimization stage, with the first scientific analyses already underway. Daily averages of the proton and alpha particle phase space density distribution functions for the whole mission is already publicly available through the *Wind* project web page. In addition, hourly resolution STICS and MASS energy spectra for select days by request throughout the mission are available in digital and

graphical formats from the University of Michigan page (<http://pooh.engin.umich.edu/wind/>). Further work is under way to produce more data products. The current status of the SMS data products is summarized in the table shown above.

### EPACT

*Documentation:* The Energetic Particles: Acceleration, Composition and Transport (EPACT) investigation consists of multiple telescopes. The highest energy telescopes (APE and IT) have failed early in the mission. However, the Low Energy Matrix Telescope (LEMT) covering energies in the 1-10 MeV/nuc range and the Suprathermal Energetic Particle telescope (STEP) measuring ions heavier than protons in the 20 keV to  $\sim 1$  MeV/nuc range still continue to provide valuable data. These instruments have been described by *von Rosenvinge et al.* [1995]. The instrument portion of this paper is reproduced at the *Wind* project web page (<http://wind.nasa.gov>). Additional instrument information is available at the instrument web page (<http://epact2.gsfc.nasa.gov/>). The newly generated sectorized count data is described also at the *Wind* project web page.

*Data Products:* Fluxes for a select number of ions (helium, oxygen, iron and combined CNO) in energy bins below 1 MeV/nuc and averaged over 92 seconds are publicly available for the whole mission in KP files at CDAWeb. As a quick look at this data reveals, the count rate of these energetic particles is very low, thus most of the KP data points are identically zero. In past, select time periods with intense particle events were manually analyzed and higher level data products generated from them. These were available on request to the public. More recently, a systematic search for events with non-zero count rates have been undertaken, and 41 such several day long periods identified in the 1997-2006 time range. For these intervals hourly resolution omnidirectional intensity data (OMN) and ion sectorized count data (SEC) were generated. These ASCII text files are publicly available at the *Wind* project web page. In addition, the first order ion anisotropy from these observations was computed. These results are also available from the *Wind* project web page. This effort will continue and more event files will be made public once the Sun becomes more active again. The current status of the EPACT data sets is summarized in the table below.

EPACT Data Product	Cadence	Coverage	Format	Location
KP fluxes	92 s	1994/11/16–Present	CDF	CDAWeb <sup>a</sup>
OMN <sup>b</sup>	1 hr	41 Events	ASCII	<i>Wind</i> Project <sup>c</sup>
SEC <sup>d</sup>	1 hr	41 Events	ASCII	<i>Wind</i> Project
Anisotropy	1 hr	39 Events	ASCII	<i>Wind</i> Project

<sup>a</sup> <http://cdaweb.gsfc.nasa.gov>;

<sup>b</sup> omnidirectional fluxes;

<sup>c</sup> <http://wind.nasa.gov>;

<sup>d</sup> sectorized counts

### MFI

*Documentation:* The *Wind* Magnetic Field Investigation (MFI) is composed of two fluxgate magnetometers located at the mid point and end of a long boom. The instrument measures DC vector magnetic fields up to a time resolution of  $\sim 22$  or  $\sim 11$  vectors/sec depending on the telemetry mode of the spacecraft. The instrument is completely described in an article by *Lepping et al.* [1995]. The instrument description sections of this paper are reproduced at the *Wind* project web page (<http://wind.nasa.gov>). Additional information on the instrument can be found at the investigation web page (<http://lepmpi.gsfc.nasa.gov>).

The data processing algorithms employed in generating the MFI data products are described by *Farrell et al.* [1995]. This paper is also available at the *Wind* Project web page. The largest source of uncertainty in the MFI data is the inherent rms noise due to averaging. The vector rms noise is computed for all data points and for all time averages from the raw telemetered resolution data and is included in the distributed data files.

*Data Products:* The MFI team essentially generates only one kind of data product, the vector magnetic fields, at various time resolutions and with increasing quality of calibrations. Within 24 hours of measurement, the 92-second KP data is publicly available at CDAWeb. This data uses periodically updated calibration tables. Typically, with no longer than 1 week delay, the MFI team produces a calibrated data product that includes 3-second, 1 minute and 1 hour averages. This data product (version 3) has the final calibrations in the spacecraft spin plane. Requiring at least of 12 months of time lag, the spin axis corrections can be computed with uncertainties of no more than a few tenths of a nT. The spin axis corrected files (version 4) are also uploaded to CDAWeb where they replace the version 3 files. Finally, after 2-3 months, all spacecraft noise effects can be included and final, archival quality data (version 5) is generated and uploaded to CDAWeb. All of these versions

have the exact same internal format. To encourage the use of the higher quality data products, CDAWeb keeps only the latest year of KP data on-line. All MFI data is backed up in the SPDF final active archive.

Till recently, the full  $\sim 11$  or  $\sim 22$  vectors/sec data was too large in volume to serve on-line and has been stored on tapes and made publicly available on request. Recently, after significant effort, the artificial spin tones were successfully reduced in this high time resolution data and was packaged in CDF format and distributed through CDAWeb and VHO.

The current status of the MFI data products is summarized in the table below.

MFI Data Product	Cadence	Coverage	Format	Location
KP	92 s	2010/09/01–Present	CDF	CDAWeb <sup>a</sup>
Versions 3 & 4 <sup>b</sup>	3 s, 1 min, 1 hr	1994/11/16–Present <sup>c</sup>	ASCII	CDAWeb, MFI <sup>d</sup>
Version 5 <sup>e</sup>	3 s, 1 min, 1 hr	1994/11/16–Present <sup>f</sup>	ASCII	CDAWeb, MFI
High Res.	$\sim 11$ or $\sim 22$ vec/sec	1994/11/16–Present	CDF	CDAWeb

<sup>a</sup> <http://cdaweb.gsfc.nasa.gov>; <sup>b</sup> Calibrated Versions 3 & 4; <sup>c</sup>  $\sim 1$  week lag; <sup>d</sup> <http://lepmfi.gsfc.nasa.gov>;

<sup>e</sup> Calibrated Version 5; <sup>f</sup>  $\sim 3$  month lag

## WAVES

*Documentation:* The *Wind* WAVES experiment composed of the RAD1, RAD2 and TNR receivers measures electric fields in a wide range of frequencies. The instrument is fully documented by *Bougeret et al.* [1995]. The instrument related sections of this paper are reproduced at the *Wind* project web page (<http://wind.nasa.gov>). Some additional documentation exists also at the WAVES instrument web page (<http://www-lep.gsfc.nasa.gov/waves/>). The content and format of the various WAVES data products are also described on the instrument web page.

*Data Products:* As most other *Wind* instruments, WAVES also produces a KP data product that is immediately publicly available at CDAWeb. The WAVES KP data contains 3-minute averages of the electric field intensities at 76 log-spaced frequencies and electron density estimates based on neural network determined electron plasma frequency values. In addition, the team produces, with no more than 1 week delay, higher time resolution (1 minute) normalized receiver voltages and makes it available both at CDAWeb and on their own web site. This is the fundamental data product that is used for the generation of the familiar WAVES frequency vs. time intensity plots. These plots are also pre-generated and publicly available on the instrument web page in PDF format. Finally, 7-10 second time resolution electron density estimates are also computed and made available at CDAWeb.

The WAVES instrument also returns short waveform captures from the time domain sampler (TDS) receiver of high frequency electric and magnetic field observations in two and three dimensions. The team is currently finalizing software that will produce all the TDS events for the entire mission to be put on CDAWeb. The data product will include all the relevant information that went into processing the final results. Each TDS event is composed of multiple channels (2 or 4, depending on the operating mode) containing either two electric field components in fast mode or three magnetic(electric) and one electric(magnetic) field components in slow mode. The data is sampled at rates between  $\sim 1875$  sps and  $\sim 120,000$  sps. The data products will be provided in CDF or ASCII format.

The WAVES team also maintains a Type II/IV catalog on their web site that is widely used. The current status of the WAVES data products is summarized in the table below.

WAVES Data Product	Cadence	Coverage	Format	Location
KP	3 min	1994/11/10–Present	CDF	CDAWeb <sup>a</sup>
TNR <sup>b</sup> , Rad1, Rad2 <sup>c</sup>	1 min	1994/11/10–Present	ASCII, IDL Save	CDAWeb, WAVES <sup>d</sup>
High Res. $n_e$ <sup>e</sup>	7-10 s	1994/11/10–Present	CDF	CDAWeb
Radio Plots	1 min	1994/11/10–Present	PNG, PDF	WAVES

<sup>a</sup> <http://cdaweb.gsfc.nasa.gov>; <sup>b</sup> Thermal Noise Receiver; <sup>c</sup> Radio Receiver Band 1, 2;

<sup>d</sup> <http://www-lep.gsfc.nasa.gov/waves/>; <sup>e</sup> electron number density

*Software Tools:* Unlike the other *Wind* instrument teams, the WAVES team distributes primarily the lowest level data they have without generating many higher level products. Therefore, dedicated software tools are necessary for non-specialists to make use of this data. The team maintains a small IDL software library on their web site that readily ingests the downloaded IDL save files and allows the custom generation of data plots.

**KONUS and TGRS**

The KONUS and TGRS  $\gamma$ -ray instruments are not maintained by heliophysics. Their data production and data distribution is completely handled by the astrophysics division. Description of the instruments and links to their data products can be found at (<http://heasarc.gsfc.nasa.gov/docs/heasarc/missions/wind.html>).

***Wind* and VHO**

Members of the *Wind* instrument teams have taken leadership roles in the development of the Virtual Heliospheric Observatory (VHO) (<http://vho.nasa.gov>). Aside from assuring that the various data products are publicly open, the most effort went into the generation of SPASE dictionary based and VHO compliant metadata. In fact, the first *Wind* data product metadata files have been used to refine the SPASE dictionary for fields and particles data. Currently, all primary *Wind* data products are fully searchable via the VHO.